Contract No:

This document was prepared in conjunction with work accomplished under Contract No. DE-AC09-08SR22470 with the U.S. Department of Energy.

Disclaimer:

This work was prepared under an agreement with and funded by the U.S. Government. Neither the U. S. Government or its employees, nor any of its contractors, subcontractors or their employees, makes any express or implied: 1. warranty or assumes any legal liability for the accuracy, completeness, or for the use or results of such use of any information, product, or process disclosed; or 2. representation that such use or results of such use would not infringe privately owned rights; or 3. endorsement or recommendation of any specifically identified commercial product, process, or service. Any views and opinions of authors expressed in this work do not necessarily state or reflect those of the United States Government, or its contractors, or subcontractors.

Metallic and Hybrid Nanostructures: Fundamentals and Applications

Simona E. Hunyadi Murph,[1*] Katie J. Heroux,[1] Charles E. Turick,[1] Darrell Thomas[2]

[1]*Savannah River National Laboratory, Savannah River Site, Aiken, SC 29860*

[2]*Oak Ridge National Laboratory, Oak Ridge, TN 37830*

*****Corresponding author, email address:* Simona.Murph@srnl.doe.gov;

Phone: 803-646-6761

Abstract. This book chapter presents an overview of research conducted in our laboratory on preparation, optical and physico-chemical properties of metallic and nanohybrid materials. Metallic nanoparticles, particularly gold, silver, platinum or a combination of those are the main focus of this review manuscript. These metallic nanoparticles were further functionalized and used as templates for creation of complex and ordered nanomaterials with tailored and tunable structural, optical, catalytic and surface properties. Controlling the surface chemistry on/off metallic nanoparticles allows production of advanced nanoarchitectures. This includes coupled or encapsulated core-shell geometries, nano-peapods, solid or hollow, monometallic/bimetallic, hybrid nanoparticles. Rational assemblies of these nanostructures into one-, two- and tri-dimensional nano-architectures is described and analyzed. Their sensing, environmental and energy related applications are reviewed.

1. Introduction:

The evolution of humans is intimately connected to the history and use of materials. Since ancient times, *Nature* provided humans with an exceptional selection of amazing materials. Surprisingly, their assortment and abundance is still deficient in the modern world.[1] As a result, scientists are continuously driven to discover new and improved materials that can potentially ensure a sustainable and higher quality of life for generations to come. Today, scientists are able to explore and understand the world at its smallest level, the atom. The first speculation on the possibility to manipulate individual atoms was introduced by physicist Richard Feynman, in 1959. In his famous talk, "There's Plenty of Room at the Bottom", Feynman described how it might be possible to print all 24 volumes of *Encyclopedia Brittanica* on the head of a stick pin.[2] Since then, a wide variety of attractive nanoscale materials have emerged ranging from metallic, semiconductors, insulators, polymers and hybrid nanostructures.

Nanomaterials are promising components in electronic circuits, bio and chemical sensing devices, catalytic processes, photonics, drug delivery- medicine, and viable alternative sources of energy.[3] Ultimately, the promise of these technologies and applications depends on several factors: (a) the scientist's ability to deliberately manipulate matter at atomic levels and create

novel structures with unique properties and functionalities, (b) nanoscale materials production in large quantities that can be (c) rationally assembled in organized nano-architectures.

In this review we bring to light advances in synthesis, characterization, rational design in one, two or three-dimensional assemblies of metallic nanoparticles, optimized geometries for chemical sensing via SERS, photocatalytic processes for environmental implications and fuel cells and solar fuel applications as a function of particles morphology and composition. Facile and flexible synthetic approaches for creating surface-engineered nanomaterials are also described. Metal nanoparticles, particularly of silver and gold, are used as templates for creation of complex and ordered nanomaterials with tailored and tunable structural, optical and surface properties.

2. Metallic nanoparticles:

Metals have been mined and used by humans since ancient times. While the date of the first human use of metals is not known, the approximate date of the discovery or first known use of metals, e.g. Pb, As, Hg, Au, Ag, Zn, Cu, Fe, dates back in 4000-300 b.c.[4] Even colloidal metals have been used since Ancient Roman times. For example, colloidal gold was used in decorative objects such as beads, ornaments, and staining glass windows. Depending on the concentration of gold, beautiful intense shades of yellow or red can be created; aggregation of the particles produces a solution that appears blue-gray. For a long time the composition of ruby-gold color was unclear. Faraday was the first to recognize that the color was due to the minute size (finely divided) of the gold particles.[5] The brightly-colored colloidal gold nanoparticle solutions prepared by Faraday in the mid-1850's are still on display today in the Royal Institution's Faraday Museum in London.[6] In the last decades, considerable progress has been made in this area due to the developments of new instruments capable of characterizing and manipulating nanostructures. To understand materials one needs to learn about their anatomical structure. The need to determine the types of atoms that constitute their building blocks and how these atoms are arranged relative to one another is essential.

Unique photo-physical, photochemical, photo-electronic, and photocatalytic properties can occur in nanoparticle systems. Nanoparticles have high surface to volume ratio that leads to structural and electronic changes that, in turn, induce other properties to become different from that of the bulk. Their properties critically depend on particle size, shape, and surface characteristics. Inorganic nanoparticles' unique properties result from their size being smaller than the mean free path of their electrons (10-100 nm) or scattering length (this length is the average distance an electron travels before being scattered).[1,6,8,10,11] At these scales new physics or chemistry occurs. For example, the bright colors observed in metal particles are due to the plasmons, which are collective oscillations of electrons in the conduction band that are excited by light of appropriate frequencies. Noble metals are extremely stable in the bulk but they are extremely "active" in the nanometer regime. At the nanometer scale, particles have a very high surface energy that makes them extremely reactive, and most systems undergo aggregation without protection or passivation of their surfaces. For example, gold is inert in its bulk form, but as a nanoparticle of ~ 3 nm it catalyzes CO to CO_2.[7]

In the case of semiconductors, their optoelectronic properties vary with nanocrystallite size. This is due to the quantum mechanical confinement of charge carriers that occurs in the 1-

10 nm regime.[8] Lower melting temperature, altered phase transformation behaviors and nonlinear optical phenomena have been observed in nanoparticles. With the decrease of particle size, extremely high surface area to volume ratio is obtained leading to an increase in surface specific active sites for chemical reactions and photon absorption to enhance the reaction and sorption efficiency. The increased surface area also increases surface states, which changes the activity of electrons and holes, and affects the chemical reaction dynamics in semiconductors. For instance, the constant of charge carrier transfer rate is relatively higher in nanoparticles than in bulk. When particle size decreases below the Bohr radius of the first excitation state, quantum size effect could occur due to the confinement of charge carriers. The quantum size effect splits both conduction and valence bands into discrete electronic states and the size dependence of optical and electronic properties becomes much more pronounced.[8] Finally, nanoparticles can induce the possibility of indirect electron transitions at the boundary of the crystals and realize the essential enhancement of light absorption. The more surface are the more active points and faster chemical reactions thus increasing the efficiency while decreasing the cost of devices and platforms.

By simply controlling nanocrystal size, shape and surface chemistry one can precisely tune their optoelectronic properties and functionalities. The particle shape and size can affect not only the activity but also the selectivity of catalysts, in the case of bimetallic colloids and/or anisotropic catalysts. Our group reported earlier the critical sensitivity of the nanoscale shape of a catalyst particle toward the oxygen reduction reaction (ORR) and methanol oxidation reaction MOR activities for direct methanol fuel cells.[9]

Nanoparticles interact strongly with light waves, even though the wavelength of the light may be much larger than the particle. They are quite different from the same materials in the bulk, which do not exhibit quantum effects. In metal nanoparticles, "plasma oscillations" driven by external electromagnetic fields are localized and lead to strong resonances at specific wavelengths that are dependent on the particle size, shape and the local dielectric environment; these effects are ultimately responsible for the brilliant colors of colloidal nanoscale gold. In the case of gold and silver nanoparticles, the plasmon bands are in the visible and near-infrared region of the electromagnetic spectrum, and are extremely sensitive to particle size, shape and local dielectric constant (Figure 1).[10,11] Nanospheres only show one plasmon band, but anisotropic shapes such as nanorods or nanowires display two plasmon bands, one corresponding to light absorption along the short axis of the nanoparticle (the "transverse" plasmon band) and another corresponding to light absorption along the long axis of the nanoparticle (the "longitudinal" plasmon band). Their plasmon bands are tunable as a function of nanoparticles size, shape, aspect ratio, aggregation state, and local environment (Figure 1).[5,6,8,9,10,11,13] In addition, particles with sharp features, such as nanorods, nanocubes, nanotriangles, etc. are expected to behave as optical antenna by concentrating the local field into a small volume.

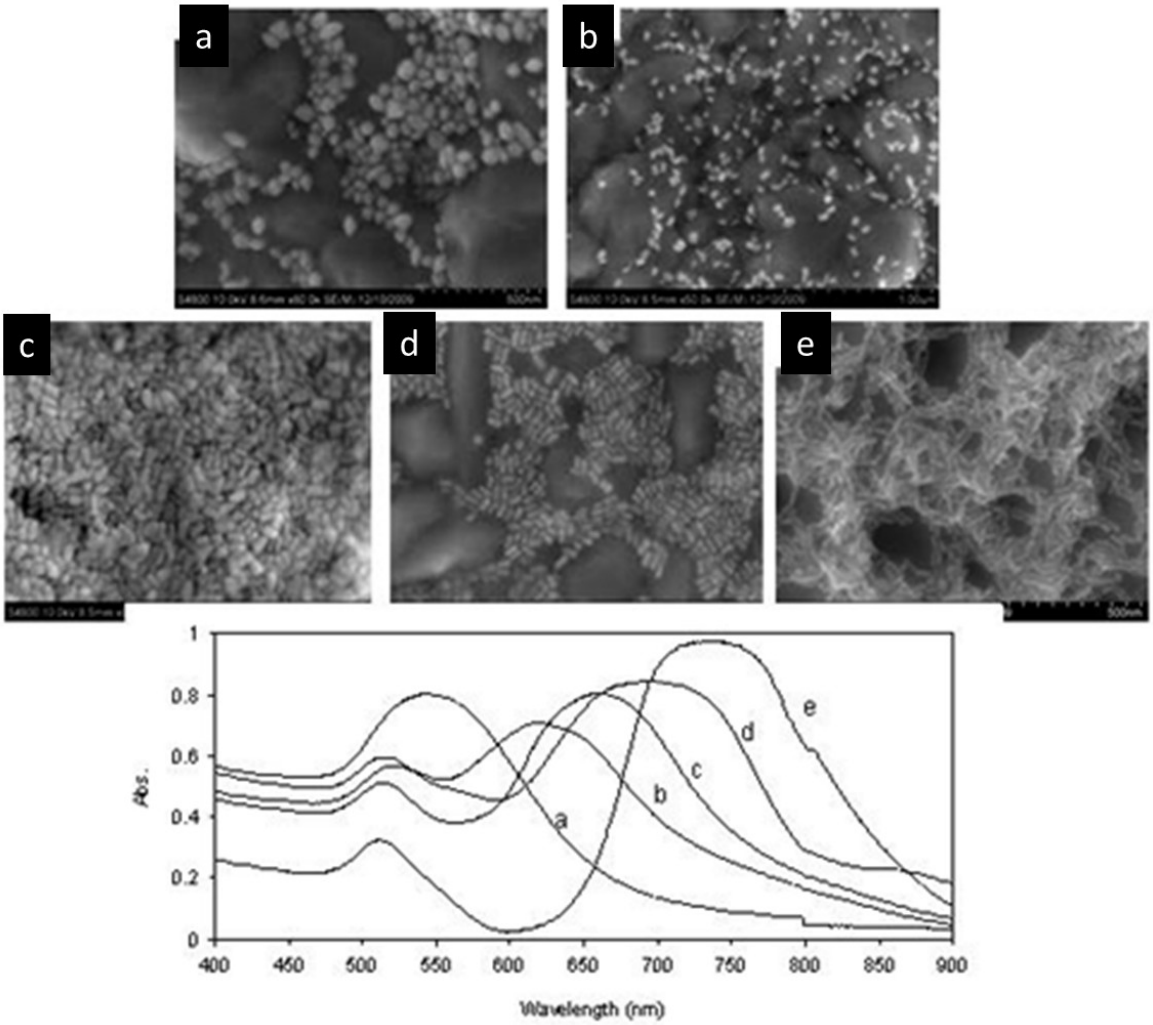

Figure 1. (a-e) SEM images of different aspect ratio (length/width) Au nanorods, from 1-5, (f) UV-Vis spectra of the corresponding Au nanoparticles.

The optical properties of nanomaterials become very important for examining surface-enhanced Raman scattering (SERS) with them. Surface-enhanced fluorescence (SEF) and surface-enhanced Raman scattering (SERS) are based on the interaction of analytes with the exceptionally strong electromagnetic field that occurs next to nanostructured noble metal surfaces in which surface plasmons have been excited.[11] Theoretical and experimental data suggests that anisotropic shapes of noble metal nanoparticles provide the most electromagnetic enhancement for surface enhanced Raman spectroscopy (SERS) and surface enhanced fluorescence (SEF), since corners and edges are "hot spots".[5,10,11] Moreover, Resonant Rayleigh scattering from metallic nanoparticles is a unique characteristic of nanoscale metals and is shape and size dependent. Depending of the nanoparticle shape various color can be obtained. These features are important for biological application when nanoparticle tracking, infiltration is necessary.[8]

Nanometer-sized particles as magnetic resonance imaging (MRI) contrast agents are particularly valuable due to ability to tune their properties (size, shape, composition, reactivity, surface area, functionalities) and direct them toward specific applications: targeted diagnostic studies, imaging/ monitoring site-specific drug delivery systems, etc. We produced for the first time novel Mn-based nanomaterials that can provide improved relaxivity and increased biological activity (lowed toxicity and organ/metabolic pathway specificity. In vitro MRI measurements made in agarose gel phantoms on Mn-Au nanoparticles exhibited high relaxivity (18.26 ± 1.04 $mmol^{-1} \cdot sec^{-1}$). Controlled incubation of the nanoparticles with mesenchymal stem cells (MSCs) was used to study cellular uptake of these particles and this process appeared to be controlled by the size of the nanoparticle aggregates in the extracellular solution (Figure 2). The high relaxivity and low cell mortality are suggestive of an enhanced positive contrast agent for *in vitro* or *in vivo* applications.[12]

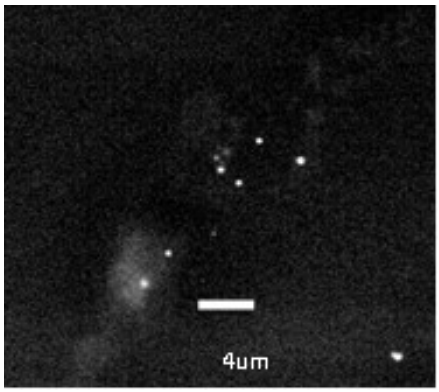

Figure 2. SEM images of live MSCs with Mn–Au nanoparticles (backscatter image). MSC is seen as the cloudy gray spot about 10 by 15 lm in while the Mn–Au nanoparticles are the multiple white spots both internal and external to the cell.

3. Synthesis procedures:

Bottom up and top down approaches are the key concepts that allows production of nanomaterials and nanoarchitectures with precisely defined properties and functions. One of the common top-down approaches to making nanomaterials is electron beam lithography which uses high voltage electrons (1 kV – 100 kV) to write nanopatterns into a resist material (ex. PMMA, ZEP-520A). E-beam lithography and atomic layer deposition (ALD) were utilized to fabricate highly ordered arrays of different shaped TiO_2 and SiO_2/TiO_2 nanoparticles supported on Si posts. These techniques allow for a great deal of size and shape control of the nanoparticles. Four-inch diameter p-type Boron-doped Si wafers coated in a positive E-beam resist (ZEP-520A) were used as the substrate for these ordered arrays. The E-beam pattern consisted of ~200 nm spheres, diamonds, squares, triangles, or rectangles in a 3x3 mm array spaced at a 2 um pitch. The exposed wafers were developed in xylenes followed by Cr-masking (~5 nm) via E-beam evaporation and acetone/isopropanol lift-off. Reactive ion etching (RIE) of the masked Si wafers

was then performed in Ar/SF6/C4F8 plasma for 6-7 min resulting in Si posts ~1 um in height. The general lithographic procedure is outlined in Figure 3.

The Si post arrays were then coated in SiO_2, TiO_2, or both via ALD (~25-50 nm). The high conformity of ALD leads to evenly coated Si posts with well-defined edges. Energy dispersive X-ray (EDX) analyses of the TiO_2 and SiO_2-TiO_2 arrays qualitatively confirmed the presence of Si, Ti, and O. The SiO_2-TiO_2 surface is known to have higher mechanical strength and thermal stability than pure TiO_2.[13],[14] Also, TiO_2 supported on SiO_2 has been shown to possess a different structure than bulk TiO_2 as well as increased photocatalytic performance.[15] The crystal structure of the TiO_2 surface also plays a role in its catalytic activity. Recent studies show that one of the most suitable phases of TiO_2 for catalytic purposes is anatase phase as it is has higher surface area and is less thermodynamically stable than the highly crystalline rutile phase.[16] At low deposition temperatures, amorphous TiO_2 films typically result as is the case in the samples prepared here by ALD at 200°C. However, studies have shown that annealing of amorphous TiO_2 films in air leads to phase transitions to its crystalline forms. Pure anatase phase is observed between 300-700°C, anatase-rutile mixture between 700-900°C, and pure rutile phase at annealing temperatures above 900°C.[17] In light of these studies, post-deposition annealing of the TiO_2- and SiO_2-TiO_2-coated post arrays fabricated herein was performed at 500°C for 2h prior to any surface functionalization or photocatalytic testing. The presence of anatase phase TiO_2 after annealing was confirmed by X-ray diffraction (XRD) analysis as compared to an as-deposited sample and a blank Si wafer.

High resolution, good alignment and high throughput ordered arrays of nanostructures of any shape can be produced by using this method. Nanolithography techniques are widely used in electronics, biotechnology, optics and photonics, various environmental and energy harvesting applications and in the fabrications of state of the art semiconductor integrated circuits and nanoelectromechanical systems. Nanolithography is an elegant technique for fabrication of nanoscale devices but large scale production is still a major concern.

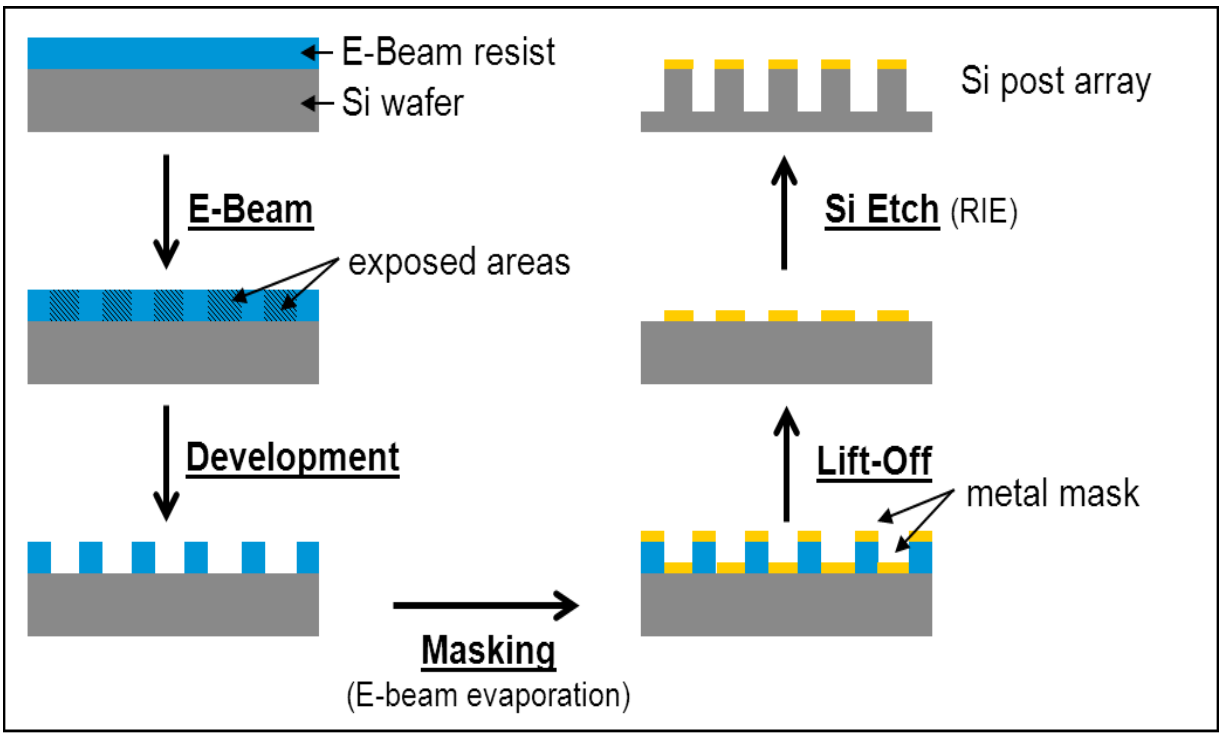

Figure 3. General fabrication procedure for ordered arrays of Si posts using electron beam lithography.

While production of nanomaterials is not a trivial task, especially at larger scales, one promising alternative strategy for production of nanostructures is a bottom up approach. A careful selection of materials and experimental procedures allow chemists to assemble atoms and molecules one at a time in a predetermined and desired matter. Since the mid-1990s an enormous amount of literature has been published with good synthetic methods to make nanoparticles of controllable size and shape (other than spheres). We have repeatedly demonstrated the ability to produce and characterize metallic nanoparticles, particularly gold, silver, platinum or bimetallic, of well-defined size, shape, aspect ratio, and monodispersity, using wet chemical approaches.[1,6,8,9,10,11,12,13,18,41]41

One of the most widely used methods for manufacturing colloidal gold, silver or platinum nanospherical particles involves the reduction of a metallic salt, e.g. chloroauric acid ($HAuCl_4$), silver nitrate, or potassium tetrachloroplatinate(II) (K_2PtCl_4), to neutral metals, Au(0), Pt(0), Ag (0), by reducing agents, such as sodium citrate or sodium borohydride. Nanospherical particles of different sizes and properties can be easily produced by manipulating the ratios between the metal ions and the reducing agents (Figure 4).

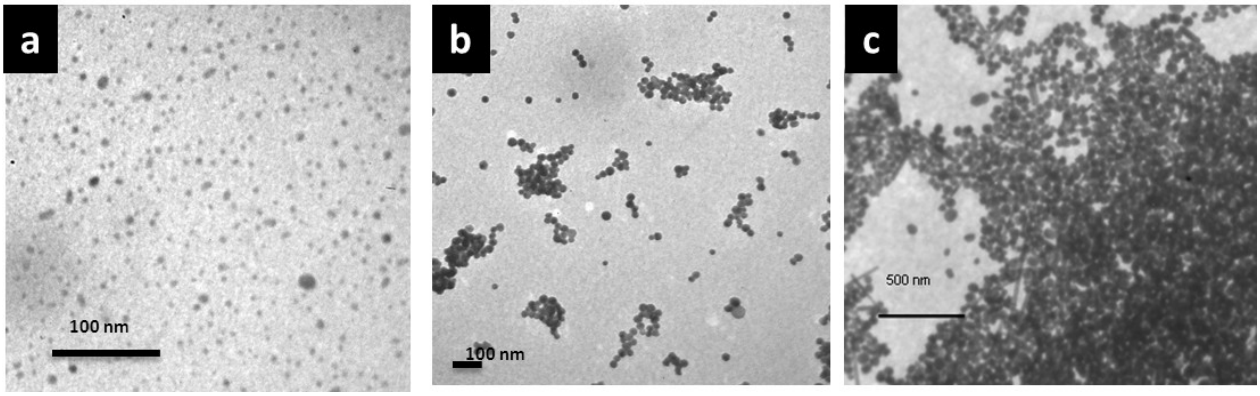

Figure 4. Various sized Au nanospheres (a) 4nm, (b) 20 nm and (c) 50 nm.

Anisotropic metallic nanostructures, e.g. rods, wires, cubes, stars, triangles, can also be produced by wet chemical procedures.[13] A seed-mediated chemical approach is used in our group to produce tunable anisotropic nanostructures (Figure 5) originally pioneered by Murphy's group.[6,8,10,13] Initially, a gold salt ($HAuCl_4$) is reduced with a strong reducing agent (sodium borohydride) to yield 3.5-4 nm spherical Au "seed" particles. The reaction takes place in water under ambient conditions. In the next step, growth solutions containing more gold salt, a structure-directing agent (cetyltrimethylammonium bromide, CTAB), and a weak reducing agent (ascorbic acid) are added to the seed particles. The ascorbic acid by itself and at room temperature is not capable of fully reducing the gold ion to the metal; but upon addition of the seeds, the reaction is thought to take place on the Au seed particle surface and produce larger nanoparticles. CTAB is the structure directive reactant that controls production of nanorod structures as opposed to larger nanospheres. The role of additive metal ions (e.g., silver ion (Ag^+)) is also critical for controlling nanorod growth. The presence of 5% Ag^+ raises the yield of gold nanorods to nearly 100%, compared to 20-40% in the absence of Ag^+. The highest aspect ratio (length to width) gold nanorod obtainable with Ag^+, however, is about six, with 95-99% monodispersity in size and shape.[5,8,9,10,11,13]

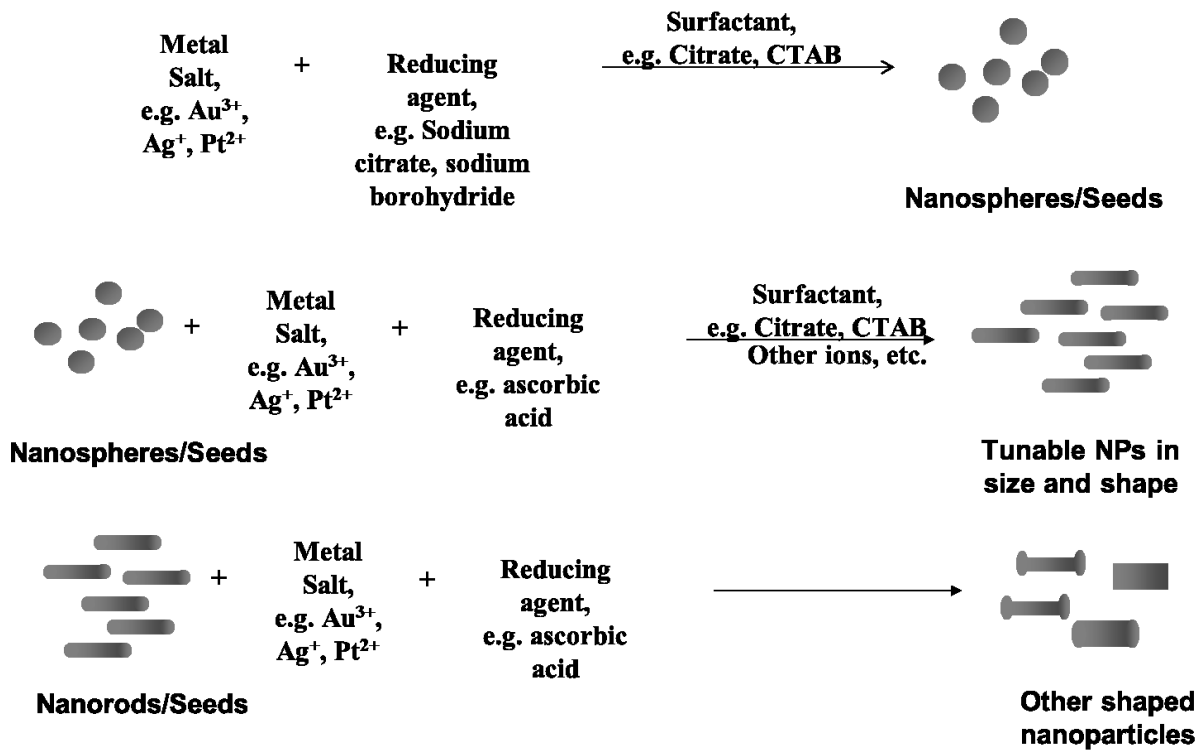

Figure 5. Schematic representation of the seed mediated synthetic routes to produce tunable in size and shape nanoparticles.

A careful selection of the nano-seeds composition, size, shape and morphology produces bimetallic nanostructures. For example, Au–Pt nanoparticles of various size, shape and aspect ratio were synthesized by the seed-mediated approach while using Au nanoparticles as seeds.[9,13] These include hexagons, cubes, blocks and tunable dog-bone nanostructures (Figure 6). The resulting bimetallic nanostructures display novel electronic, optical and catalytic properties distinct from their template nanoparticles. A rotating disk electrode was used to evaluate electrochemical performance of these Au–Pt nanocatalysts in the oxygen reduction reaction (ORR) and the methanol oxidation reaction (MOR) of direct methanol fuel cells. While Au in the samples seems to lower the performance for the ORR, great benefits are observed in the presence of MeOH and O_2. Depending on the geometry and the Pt/Au ratio, Pt-based catalysts can be prepared that reduce and, in some cases, eliminate the detrimental effects of methanol crossing over to the cathode. The results indicate the Au–Pt dogbones are partially and in some cases completely unaffected by methanol poisoning during the evaluation of the ORR. The ORR performance of the octahedron particles in the absence of MeOH is superior to that of the Au–Pt dogbones and Pt-black; however, its performance is affected by the presence of MeOH.[9]

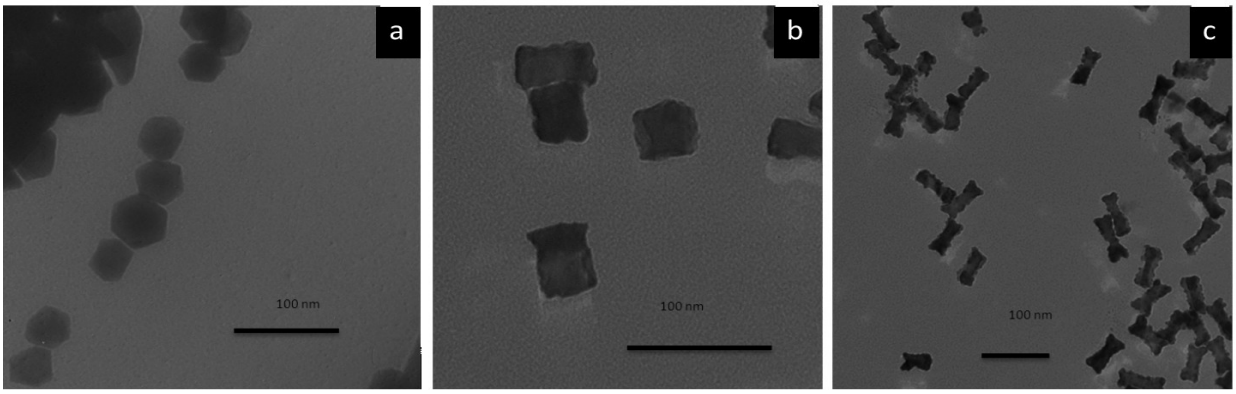

Figure 6. TEM images of Au-Pt (a) hexagons, (b) blocks and (c) dog-bones.

Another procedure perfected by our group to prepare one-dimensional silver nanostructures is a seedless, sufactantless approach.[13,18,31] High aspect ratio silver nanowires with lengths from 0.5 micron to 20 microns and 30 nm in diameter can be produced by boiling silver nitrate aqueous solutions in the presence of sodium citrate, and sodium hydroxide (Figure 7. One of the benefits of these nanostructures arises from their "surfactant free" surface.

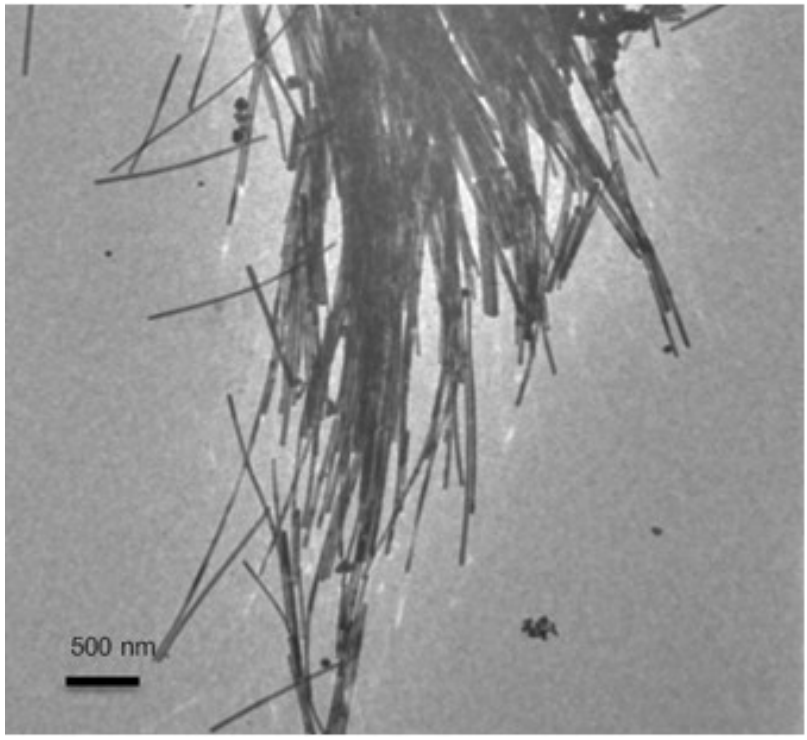

Figure 7. TEM image of Ag nanowires.

Galvanic replacement reactions have been used to good effect to synthesize hollow gold nanomaterials starting from these silver nanomaterial precursors.[6,11] This reaction is spontaneous based on their reduction potentials: Ag^+/Ag^0 has a standard reduction potential Eu =+0.8 V, and the analogous potential for $AuCl_4^-/Au^0$ is +0.99 V.[11]

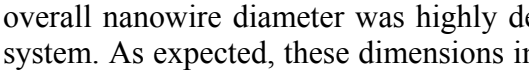

$$3\ Ag\ (s) + HAuCl4\ (aq) \rightarrow Au\ (s) + 3\ AgCl\ (aq) + HCl\ (aq)$$

The initial morphology of the Ag nanowires was preserved during the galvanic replacement reaction. The size of the growing Ag-Au and Au hollow core was determined by the original diameter of the silver nanowires, around 30 nm. The average diameter and wall thickness was easily tuned from 10 to 30 nm (wall) and 40–70 nm (diameter) (Figure 8 a).[11] The overall nanowire diameter was highly depends on the Au salt metal concentration added to the system. As expected, these dimensions increased when the Au concentration increases. The UV-Vis spectra of the newly produced bimetallic Au-Pt or Au hollow nanotubes differ not just from the monometallic colloids but are also highly dependent on the nanotube's composition. The continuous red shift of the silver nanowire transverse plasmon band, originally at ~400 nm, confirms the formation of bimetallic colloids and that the materials are not just mixture of pure silver and pure gold nanoparticles (Figure 8b). The longitudinal plasmon-band of the silver nanowires is beyond 1200 nm. EDX confirmed the composition of the final product, which are gold nanotubes (Figure 8c).

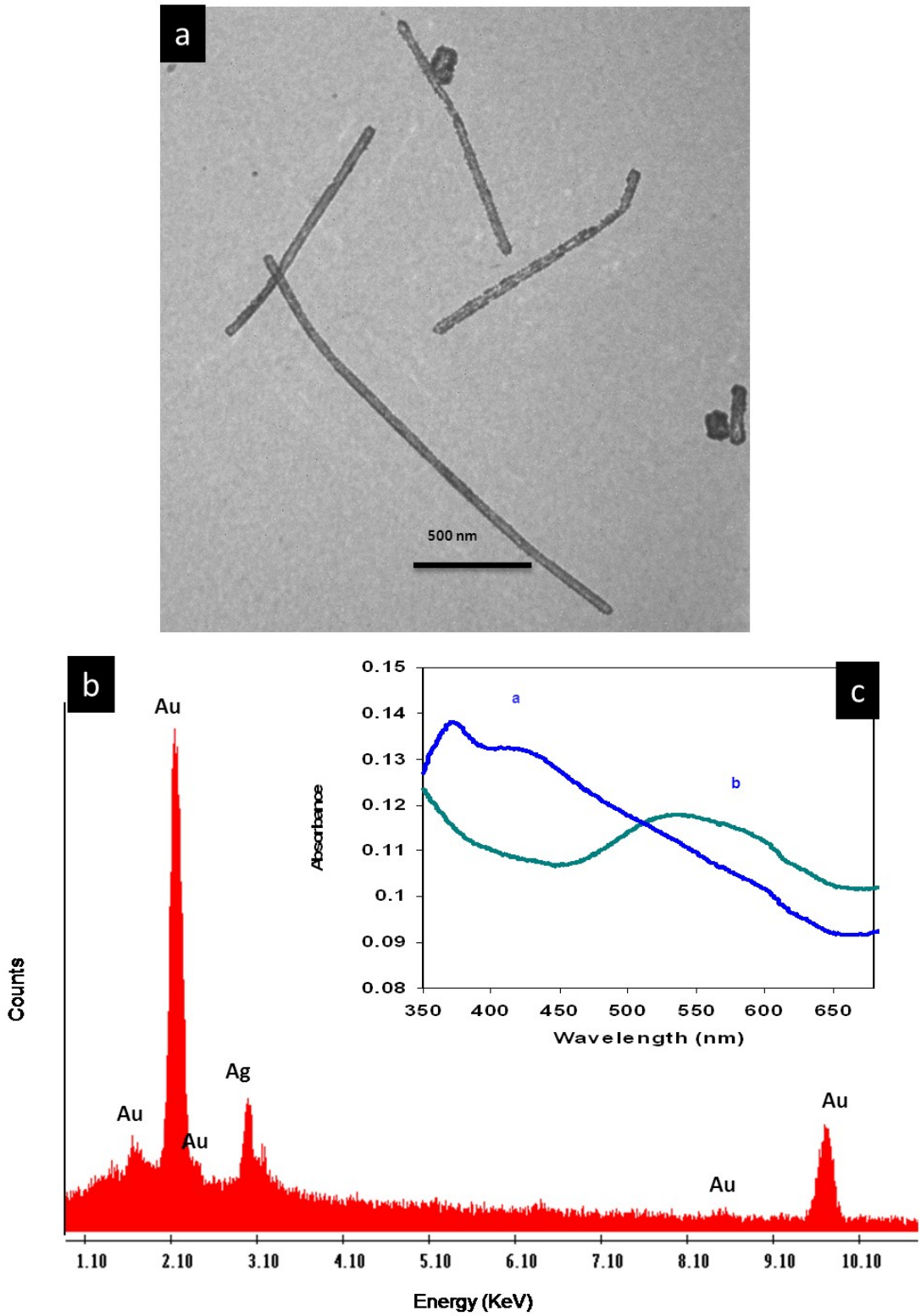

Figure 8. (a) TEM image of Au-Ag hollow nanotubes, (b) UV-Vis spectra of Ag nanowires (blue) and Au nanotubes (green), (c) EDX of Au nanotubes.

4. Rational assemblies of metallic nanoparticles

Rational assemblies of metallic nanoparticles in one-, two- or three dimensions have become an increasingly attractive method for developing nanoscale architectures for electronics, sensing, and photocatalytic applications. Nanoscale architectures often exhibit improved physical and chemical properties over their single-component counterparts, and hence are potentially useful in a broader range of applications. At the nanometer scale, particles have a very high surface energy that makes them extremely reactive, and most systems undergo aggregation without protection or passivation of their surfaces. It is possible to inhibit particle coalescence during the synthesis of metal nanoparticles by a careful selection of the capping ligands, stabilizers, or polymers.[19] Surface modification of inorganic nanoparticles can also improve the interactions between nanoparticles and biomolecules or can help to target specific cells and even the nucleus.[20]

The preparation procedures and nanomaterial's properties has been described above. This section focuses on the science and engineering underlying the use nanomaterials for sensing, environmental and energy related applications. We used the following three different concepts to describe our work on one-, two- or three dimensional nanostructures and nanoarchitectures (Figure 9).

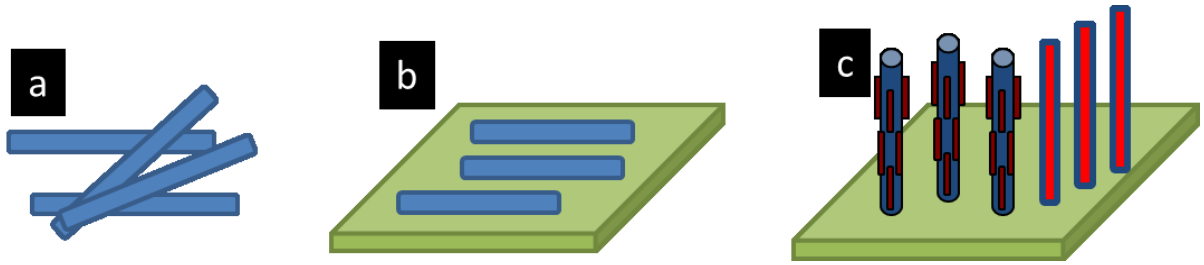

Figure 9. Schematic representation of (a) One dimensional nanostructures in aqueous solution, (b) Two dimensional nanostructures produced by parallel placement of one dimensional nanostructures on solid support and (c) Three dimensional nanostructures formed by perpendicular placement of one dimensional nanostructures on solid support.

4.1. One-dimensional nanostructures:

One dimensional nanoscale materials are gaining momentum for sensing and spectroscopic applications, particularly in SERS applications. SERS is one of the most promising optical techniques for bioanalytical applications yet not fully explored. Surface enhanced Raman scattering (SERS) is a vibrational technique in which the Raman signatures of molecules that are near metal nanoscale surfaces are greatly enhanced in intensity compared to the molecules alone.[8,10,11,21,27] This is due to the enormous electric fields created when plasmon modes are activated by absorption of visible light. Theoretical and experimental studies suggests that anisotropic shapes (rods, wires, cubes, stars, etc.) of noble metal nanoparticles (e.g. Au and Ag) can provide the most electromagnetic enhancement for SERS since corners and edges are "hot

spots".[8,10,11] Some of the key features to generating very large SERS enhancement factor are as follow:

(a) Use of SERS active nanomaterials. Gold and silver nanoparticles are excellent substrates to detect molecules with surface-enhanced Raman scattering (SERS) techniques.[6,8,11,21]

(b) Excite nanoparticles at their plasmon resonance. Anisotropic nanostructures, nanorods and nanowires, thought to be superior to nanospheres for SERS. This is because the optical properties of the particles are tunable through control of the morphology. This allows tuning of the surfaces for the excitation and Raman scattering frequencies. If the resonance between the incident radiation and the electronic absorption maxima overlap, greater SERS enhancements for these nanoparticles are reported. Also, if the molecule to be detected is located at the tips of the rods, considered "hot spots", rather than the side's additional enhancement is produced.

(c) Surface roughness of the nanometal used. The first surface-enhanced Raman (SERS) spectrum was observed in 1974 by Fleischmann *et al.*[22] for pyridine adsorbed on electrochemically roughened silver. However, Jeanmaire and Van Duyne were the first one to realize in 1977 that the Raman intensity was magnified by a factor ca. 10^6 over what was reasonably expected[23]. They proposed an electromagnetic effect for the enhancement effect while Albrecht and Creighton proposed a charge-transfer effect[24]. Today, the scientific community agrees that SERS are the results of two different effects. The electromagnetic (EM) effect is due to enhancement of the local electromagnetic field incident on an adsorbed molecule at a metallic surface. The chemical effect is due to the electronic resonance/charge transfer between a molecule and a metal surface, which leads to an increase in the polarizability of the molecule. Both processes result from the strong increase of local electromagnetic field in close vicinity to metal (i.e., silver or gold) surfaces that accompanies excitation of surface plasmon resonances in the metals.

(d) Produce nano-junction dimers (Figure 10). Large enhancement factors and even single-molecule SERS are expected for molecules at junctions between aggregated nanoparticles.[25] This is a result of localized surface plasmon (LSP) coupling between nanoparticles and enhanced electromagnetic field intensity localized at nanoparticle junctions. Nanoscale junctions between metal nanoparticles provide larger surface-enhanced Raman scattering signals for molecules that reside there, compared to single particles.[26,27] For example, Schatz *et al.* describes special silver nanoparticle array structures that lead to exceptionally large electromagnetic field enhancements ($|E|^2 > 10^7$) at specific locations in the structure, thus providing a purely electromagnetic mechanism for producing single molecule. There are numerous excellent reviews on sensing applications via SERS. The most recent reviews are a part of a special session in Chemical Reviews (2011).

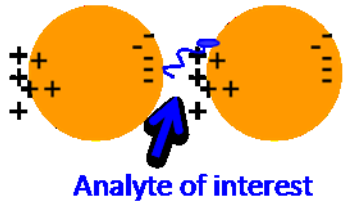

Figure 10. Schematic representation of nano-junction dimers.

Silver and gold nanoparticles have been successfully used as substrates for surface enhanced Raman sectroscopy (SERS) in colloidal solution and on solid substrates.[6,8,10,11,32] Based on the experimental conditions, such as analyte of interest (4-MBA, 4-ATP, etc), size and shape of nanoparticles, overlap of the plasmon band with laser wavelength, etc. enhancement effects of 10^4-10^9 were recorded by us.[6,8,10,11,21]

We used 4-mercaptobenzoic acid (4-MBA) as a model analyte (Figure 11). 4-MBA binds to silver and gold through the thiol group, and its ring-breathing modes are the ones seen in Table. We evaluated silver nanowires, - in colloidal solution-, as a SERS substrate for 4-MBA, and compared them to the bimetallic Ag-Au nanowires, and the gold nanotubes. Raman spectrum of pure solid 4-MBA is reported in figure. Raman spectra were acquired for 4-MBA in the presence of silver nanowires, gold–silver bimetallic nanowires, and gold nanotubes. Surface enhancement factors (EF) were calculated by using the following expression:[11,27]

$$EF = [I_{SERS}]/[I_{Raman}] \times [M_{bulk}]/[M_{ads}]$$

where M bulk is the number of molecules sampled in the bulk, M_{ads} is the number of molecules adsorbed and sampled on the SERS-active substrate, I_{SERS} is the intensity of a vibrational mode in the surface-enhanced spectrum, and I_{Raman} is the intensity of the same mode in the Raman spectrum. The intensity of the n(CC)ring ring-breathing mode at 1070 cm^{-1} was used to identify the enhancement factors. All spectra were normalized for the acquisition time. The Raman spectrum of solid 4-MBA was used in our calculation for the enhancement factor for the ‘‘bulk’’ values. As reported earlier the enhancement factor we calculate the number of molecules sampled, which depends on the surface area of each nanoparticle sample; the number of molecules estimated to be present in the illuminated volume of our laser; and the surface coverage likely for 4-MBA, assuming monolayer coverage, which is 3 molecules nm^{-2} = 0.5 mmol cm^{-2}.[11,27]

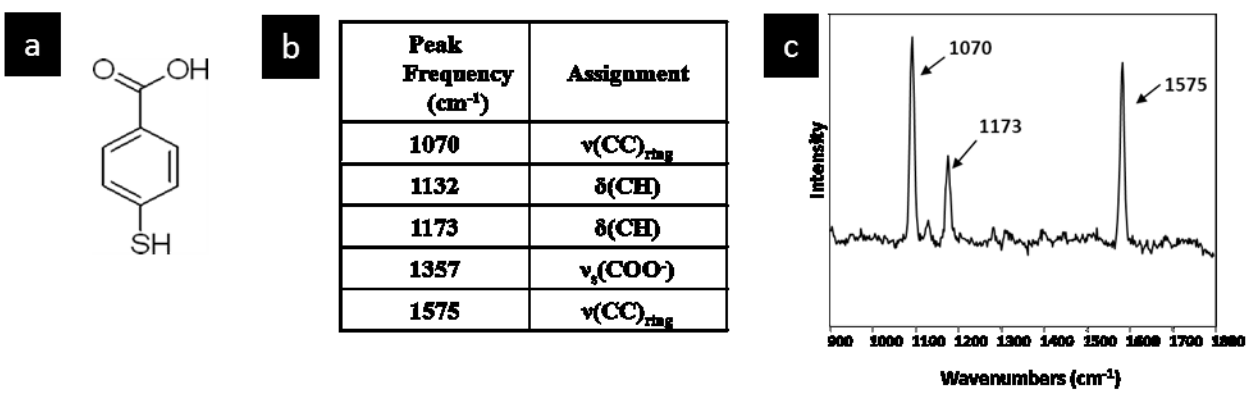

Peak Frequency (cm^{-1})	Assignment
1070	$\nu(CC)_{ring}$
1132	δ(CH)
1173	δ(CH)
1357	$\nu_s(COO^-)$
1575	$\nu(CC)_{ring}$

Figure 11. (a) Chemical structure of 4-MBA, (b) Peak frequency assignment for MBA, and (c) Normal Raman spectrum of solid 4-MBA. Reproduced by permission of The Royal Society of Chemistry

Our findings show that bimetallic nanowires provide more SERS signals than pure silver nanowires (Figure 12). Gold nanotubes, while not providing as large enhancement factors

compared to the bimetallics, are surprisingly better than solid long gold nanorods in similar colloidal SERS experiments.[11]It is believed that a better matching of the laser wavelength with the material composition, and the possible formation of pinholes in the overcoating layer which might function as SERS hot spots are responsible for these enhancements effects. Enhancement factors of 5 to 40 enhancements were recorded for bimetallic nanowires compared to silver nanowires alone.[11]

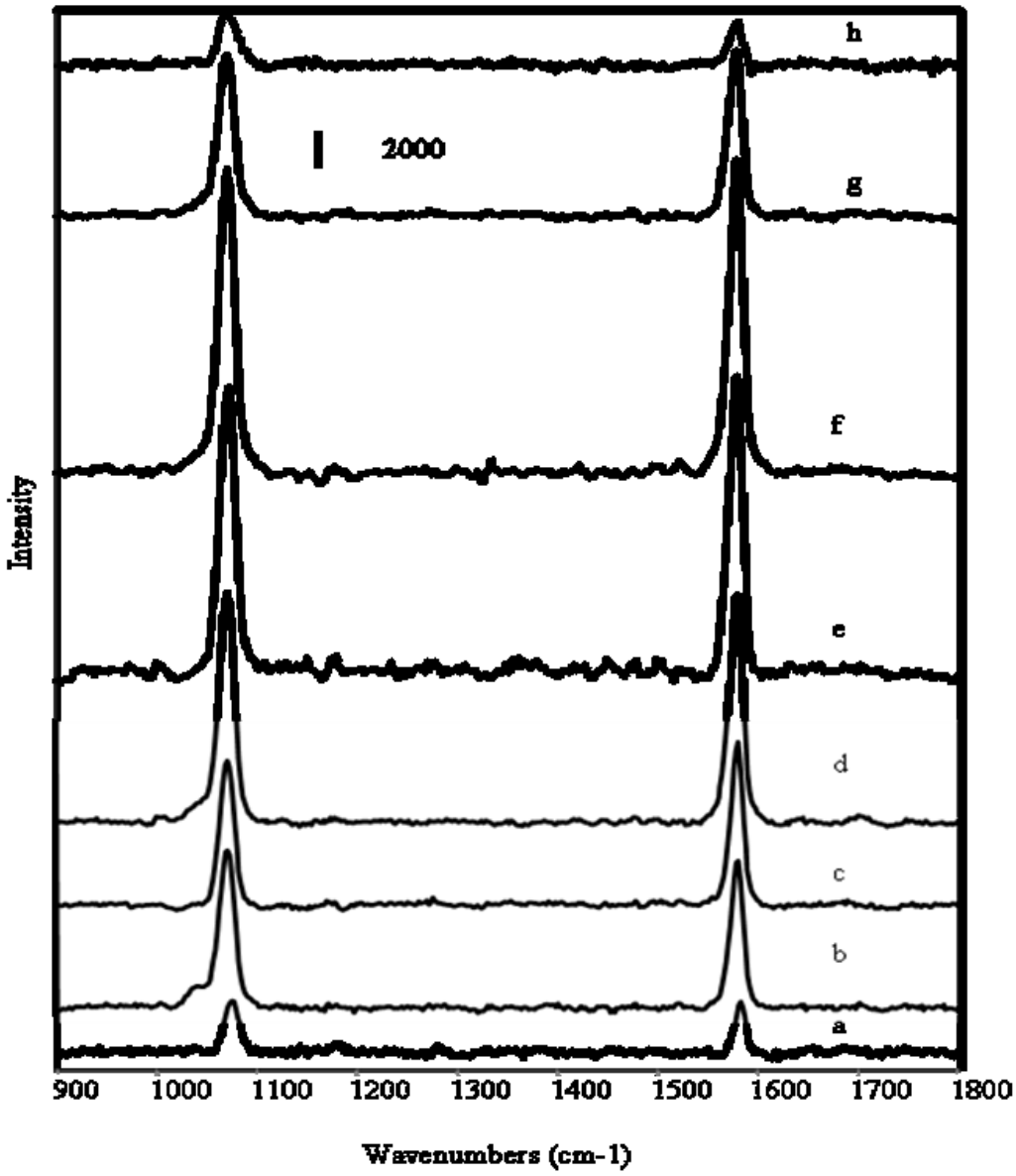

Figure 12. Surface enhanced Raman spectra of 4-MBA using (a) silver nanowires and bimetallic colloids with various wall thickness: (b) 10±1 nm, (c) 13±1 nm, (d) 17±1 nm, (e) 19 ± 1, (f) 22 ±1 nm, (g) 27±1 nm, (h) 32±1. Reproduced by permission of The Royal Society of Chemistry

Production of end-to-end assemblies or ordered arrays of nanostructures is interesting for numerous sensing or electronic applications. We have performed a series of reactions on gold and silver nanostructures for fabrication of such substrates. This includes surface functionalization, incubation in solvents, and controlled dissolution. The surface of the metallic nanomaterials can be easily engineered with a large variety of functional groups that can improve the interactions and self-assembly formation.

For example, when placed in various organic solvents, specifically methanol and ethanol end-to-end assemblies are easily produced (Figure 13). The organic solvents did not affect the original shape and size of the Au nanorods. When Au nanorods are arranged in an end-to-end manner, a red shift of the longitudinal plasmon band in the UV-Vis spectra is produced. These data show a shift in maximum extinction to longer wavelengths and the presence of additional absorption peaks. This red shift is predicted by theory based upon the influence that the dielectric constant of the surrounding medium has on the surface plasmon resonance of the nanoparticles. The additional peaks are thought to be due to a combination of solvent absorbance and changes in the particle-size distribution due to aggregation processes. Broadening of the plasmon peaks is also observed indicating clustering of nanoparticles in the organic solutions. The UV-Vis data (Figure 13ii) are in agreement with the SEM images. In particular, for the ethanol and methanol systems where end-to-end assemblies are formed, new peaks are formed in the 900-1100 nm regime. This is consistent with the notion that the longitudinal plasmon band of the nanorods along the long axis is coupling and is highly dependent on the size of the linear Au nanorods assemblies. This result is also associated with a relative decrease of the transverse plasmon band. The experimental results are in agreement with theoretical studies and other reported experimental results.[28,29]

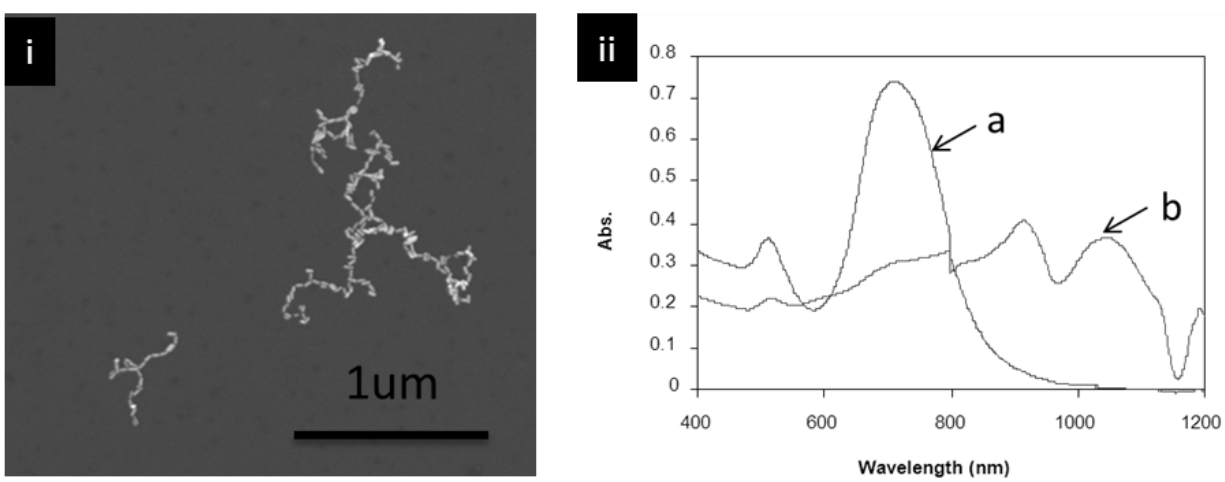

Figure 13. (i) SEM image of self-assembled Au nanorods in methanol, (ii) UV-Vis spectra of Au nanorods in (a) water and (b) methanol.

Core-shell colloidal materials are also of interest due to their applications in sensing (SERS/SEF), catalysis, diagnostics, decorative materials, and nanoscale electronic devices.[30] In view of these applications we fabricated a wide arrays of core-shell Au-silica, Ag-silica, Au-silica-titania, etc. nanoarhitectures.[31,32] We have reacted CTAB-coated gold nanorods and citrate-coated Ag nanowires with mercapropropyltrimethoxysilane ($HS(CH_2)_3Si(OCH_3)_3$) to form Au-S bonds and leave the trimethoxysilane group facing the solvent. Subsequent reaction with sodium silicate forms a SiO_2 layer around the gold or silver particles. We can control the thickness of the silica layer from ~5-150 nm. TEM is used to visualize the shells (Figure 14).[6,31]

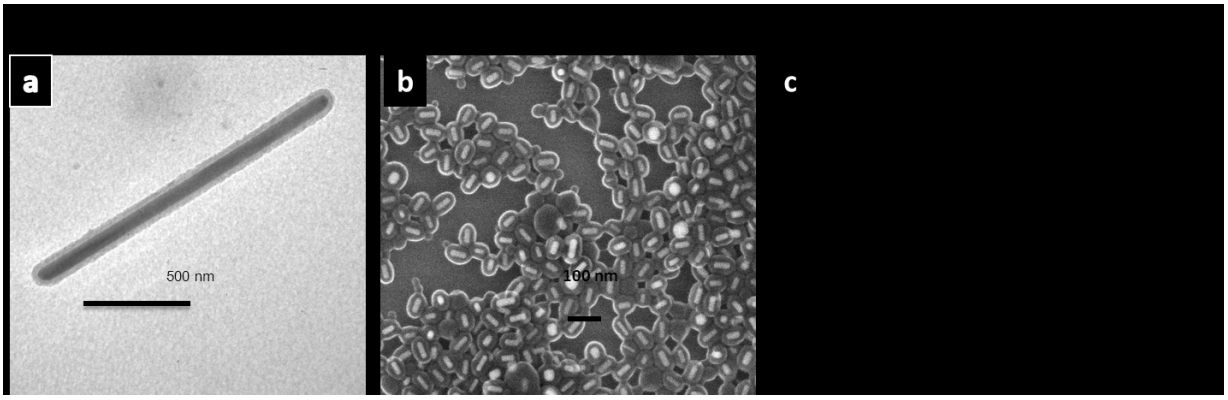

Figure 14. (i, ii) SEM images of Ag-silica nanowires with tunable silica shell, (iii) UV-Vis spectra of Au and Au-silica rods; inset SEM image of Au-silica core-shell nanorods.

Zeta potential analysis is used to confirm the effective surface charge of the particles. Initial Au nanorods have a positive +33±2mV surface charge due to the CTAB coating, while Ag nanowires have a negative surface charge of -45±4mV due to either citrate or hydroxide ions present on the surface. The effective surface charge after silica shell coating was negative after silica coating, -57±2mV for Ag nanowires coated with a 50 nm silica shell.[1,6,10,13,18] Coating the nanoparticles with different materials that have very different dielectric constants shifts the position of the plasmon bands in ways that are readily identifiable spectroscopically and theoretically understood. These nanostructures are further exploited for production of "nanopeapod" architectures in which silver "peas" are embedded in a silica "pod".[1,31] The dimensions of the peas, and their spacing within the pod, are controllable on the nanoscale.

Periodic arrays of metallic structures (specifically, lithographically-prepared silver nanorods) embedded in dielectric media are able to guide and modulate light transmission (even through corners and tee structures) in a regime dominated by near-field coupling.[31,56] Recently, peapod-like structures were prepared by Wiley's group[33] by scrolling of niobate nanosheets (NSs) in the presence of magnetic nanoparticle (NP) chains. $Pt@CoAl_2O_4$ inorganic peapod nanostructures consisting of well-defined Pt NPs encapsulated in continuous $CoAl_2O_4$ nanoshells, were realized by electrodeposition of cobalt/platinum multilayered NWs into nanoporous anodic aluminum oxide membranes and subsequent solid-state reaction at high temperature.

Moreover, by using modification of the silica coating work reported above,[18,32] 4-MBA was captured onto Ag nanowires, in colloidal solutions, with patchy or full silica deposits to examine their relative abilities for Raman scattering experiments (Figure 15, Table 1). Through an ammonia treatment we produced "nano-matryoshka" configurations consisting of concentric nanowires/nanotubes of metal/insulator nanomaterials.[32] The metallic inner nanoparticle is made of an undersized (as a result of the reaction between Ag and ammonia) Ag nanowires functionalized with 4-MBA while the outer shell, the insulator, is the original, now oversized silica shell.[32] All these configurations were used to quantitate/explore the effect of the electromagnetic field at the tips of the nanowire ("hot spots") in the Raman scattering experiment. [6,11,18] Surprisingly, out of all of these silica-silver nanoarchitectures, patchy coats of silica on silver nanowires produce by far the largest signal for 4-MBA. This suggests that the electromagnetic enhancement is associated with the substrate dielectric properties of the surrounding medium. It has been reported earlier that the tip of metallic nanoparticle can be considered as a local electromagnetic source[34] which create an enhancement effect in SERS. Theoretical analysis indicates that the electrochemical potential may affect the absorption spectrum and surface-enhanced Raman scattering experiment.[35] The surface dielectric constant depends on the surface morphology. Schatz presented a model for determining the enhancement of local electromagnetic fields which occurs close to metal surfaces through surface plasmon excitation. This model considers a random distribution of metal hemispheroids on a perfectly conducting flat plane. He concluded that surface roughness contributes 10^2 to 10^3 to the overall enhancement with a frequency dependence which is close to that seen experimentally.[36]

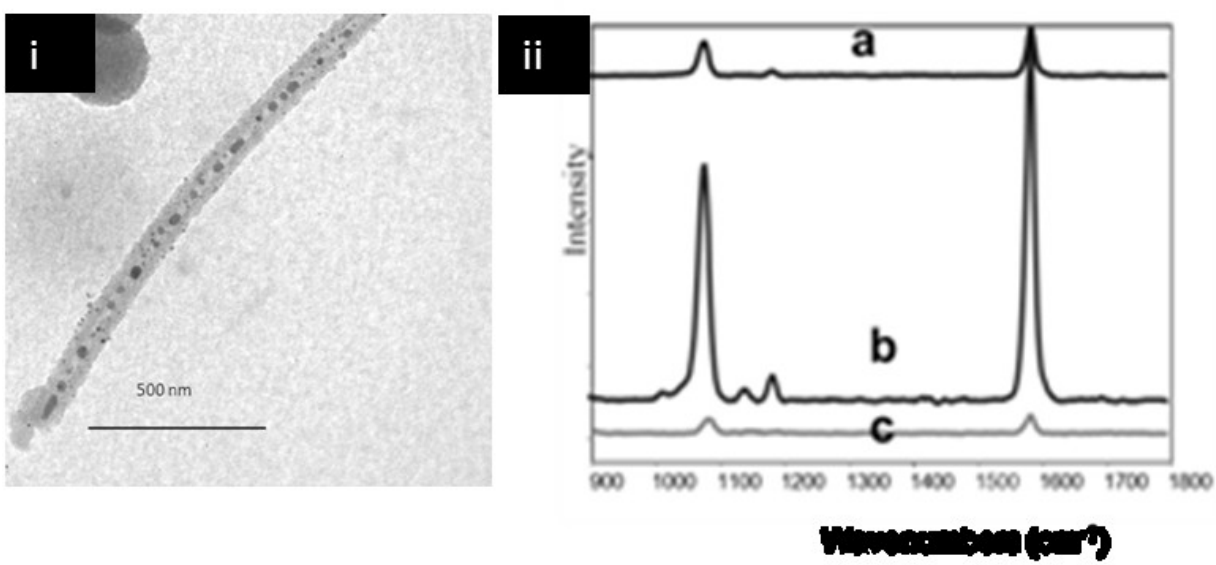

Figure 15. (i) TEM image of Ag-silica nanopeapods and (ii) Raman spectra of (a) Ag nanowires, (b) patchy silica coatings onto Ag nanowires and (c) full silica coatings onto Ag nanowires.

Table 1. Substrates used for SERS experiments.

Substrate	Cartoon Image	TEM image	Calculated EF
a. Silver nanowires		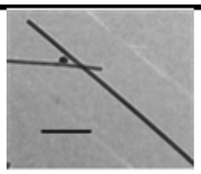	$1.1 \pm 0.3 \times 10^{6}$
b. Patchy Silica coatings onto Ag nanowires		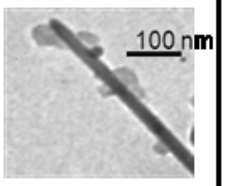	$6.5 \pm 0.4 \times 10^{8}$
c. Full silica coatings onto Ag nanowires		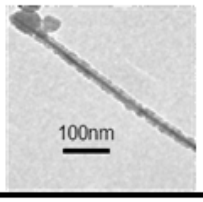	$2.8 \pm 0.3 \times 10^{6}$
d. Nano-matryoshka architecture		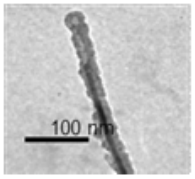	$2.9 \pm 0.6 \times 10^{6}$
e. Nano-peapod architecture		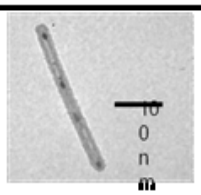	$1.3 \pm 1.5 \times 10^{7}$

Whether through electrostatic or covalent bonding, nanoparticles can self-assemble to form secondary architectures with properties dictated not only by those of the individual building blocks but also by the spatial arrangement and coupling interactions between them. The gold nanoparticles have a positive surface charge due to the CTAB surfactant bilayer whereas the CNTs have an intrinsic negative surface charge. Simply mixing solutions of these two species together in the appropriate solvents can lead to electrostatic assembly of the Au nanoparticles on the CNT surface. Furthermore, bifunctional linkers can be used to covalently attach Au nanoparticles to CNTs by exploiting the strong affinity of Au for thiol or amino groups. These general approaches are shown schematically in the top of Figure 16. SEM images (bottom of Figure 16) show the alignment of Au nanospheres and nanorods along the surface of the CNTs. Though aggregation of the CNTs in certain solvent conditions was problematic, the attachment of the Au nanoparticles is clearly shown in these images. Furthermore, the absorption spectra of these self-assembled materials showed a significant red shift in the longitudinal plasmon band indicative of plasmonic coupling between neighboring Au nanoparticles. Such self-assembled nanoparticles have gained widespread attention in the areas of electronics, photonics/plasmonics, biological and chemical sensing, and catalysis.

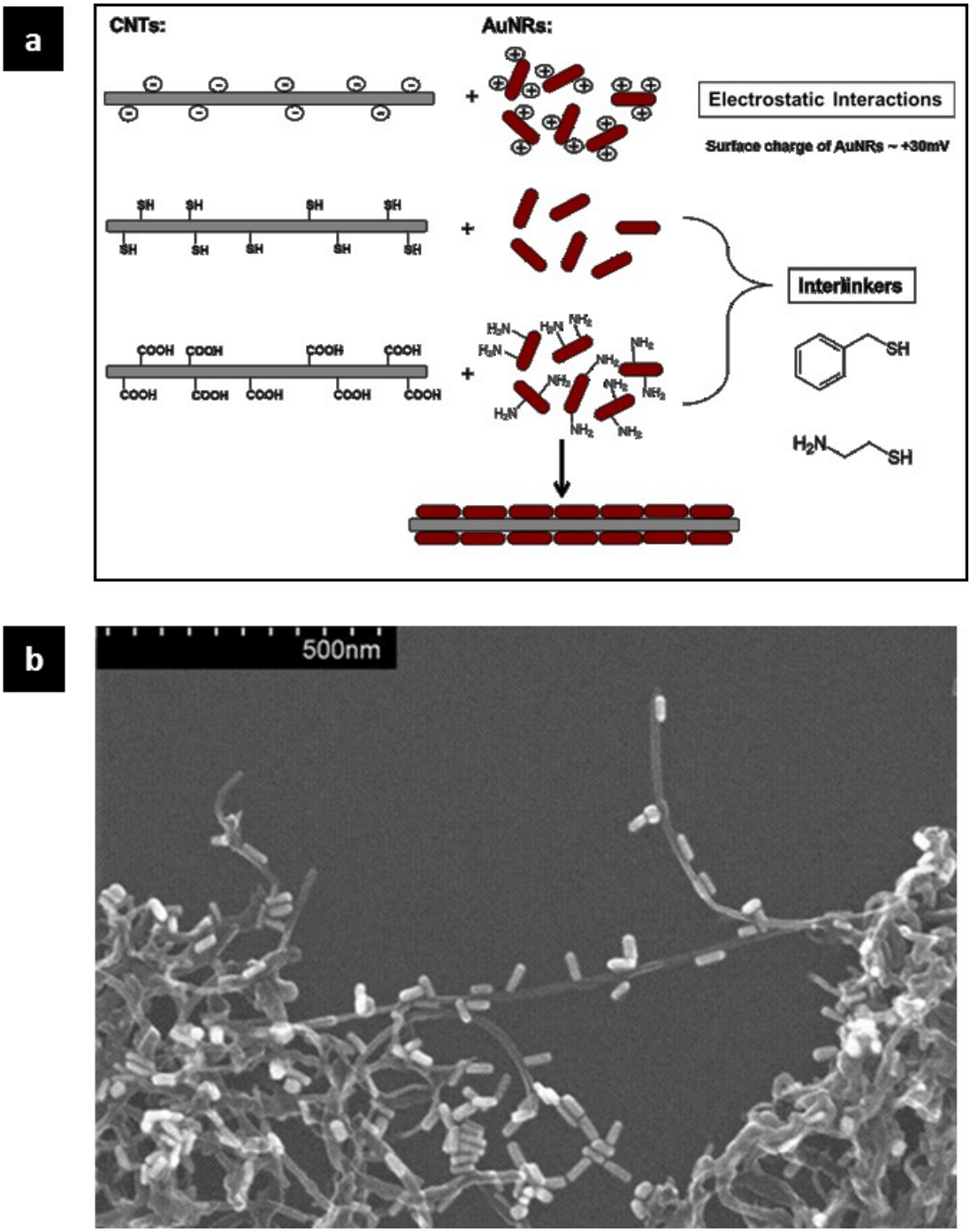

Figure 16. (a) Schematic representation of attachment of AuNRs to CNTs through electrostatic or covalent linkages; (b) SEM images of Au and rods self-assembled on the surface of CNTs.

4.2. Two-dimensional nanostructures:

Spontaneous assemblies of iron oxide nanoparticles were reported for the first time in 1989.[37] A drop-casting approach followed by solvent evaporation allows creation of uniquely patterned assemblies. The self-assembly process is the result of the physico-chemical properties and structural affinities of the nanoparticle's building blocks. The combination of solvent evaporation from the sample drop and interfacial hydrophilicity or hydrophobicity as well as the balance between van der Waals, capillary, surface tension, hydrophobic, or electrostatic interactions, etc is responsible for a variety of assemblies and agglomeration features (agglomeration, end-to-end, end-to-side, etc).

Nanoparticles prepared in solution are often capped with a variety of surfactant or capping agents used during the preparation procedures, including citrate, CTAB, PVP, etc. This provides surface passivation and helps prevent aggregation of nanoparticles. Cationic surfactants such as CTAB, when present as surface-adsorbed multilayers, are known to induce self-ordering of spherical gold nanoparticles.[38] This is believed to be due to a balance between the short-range electrostatic repulsion between the metal core of the nanoparticle and interchain attractions between the CTAB tails. It is also reported that, upon concentration from an aqueous solution, this process can lead to higher order structures with gold nanorods of aspect ratio 4.6 being produced in systems containing two different cationic surfactants.[39] The convective forces due to solvent evaporation along with Van der Waals forces, capillary forces, surface tension and others are all accountable for creation of nanoparticle assemblies. As prepared, the gold nanospheres and nanorods have either citrate or CTAB coatings (Figures 17). FTIR, thermogravimetric analysis data, and zeta potential analysis support the notion of the CTAB bilayer depicted below.[68,10,26]

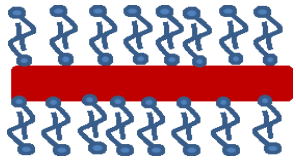

Figure 17. Schematic representation of Au nanorods coated with CTAB surfactant.

We and others[40] investigate self-assemblies processes by using anisotropic gold nanoparticles. When gold nanorods were air-dried on copper grids, they tend to orient in various side-to-side or end-to-end architectures (Figure 18). Micrometer size domains of parallel-, linear-aligned or other unique arrangements can be observed. These unique architectures are highly dependent on a variety of experimental conditions, including Au nanoparticle concentration, solvent, temperature, etc.

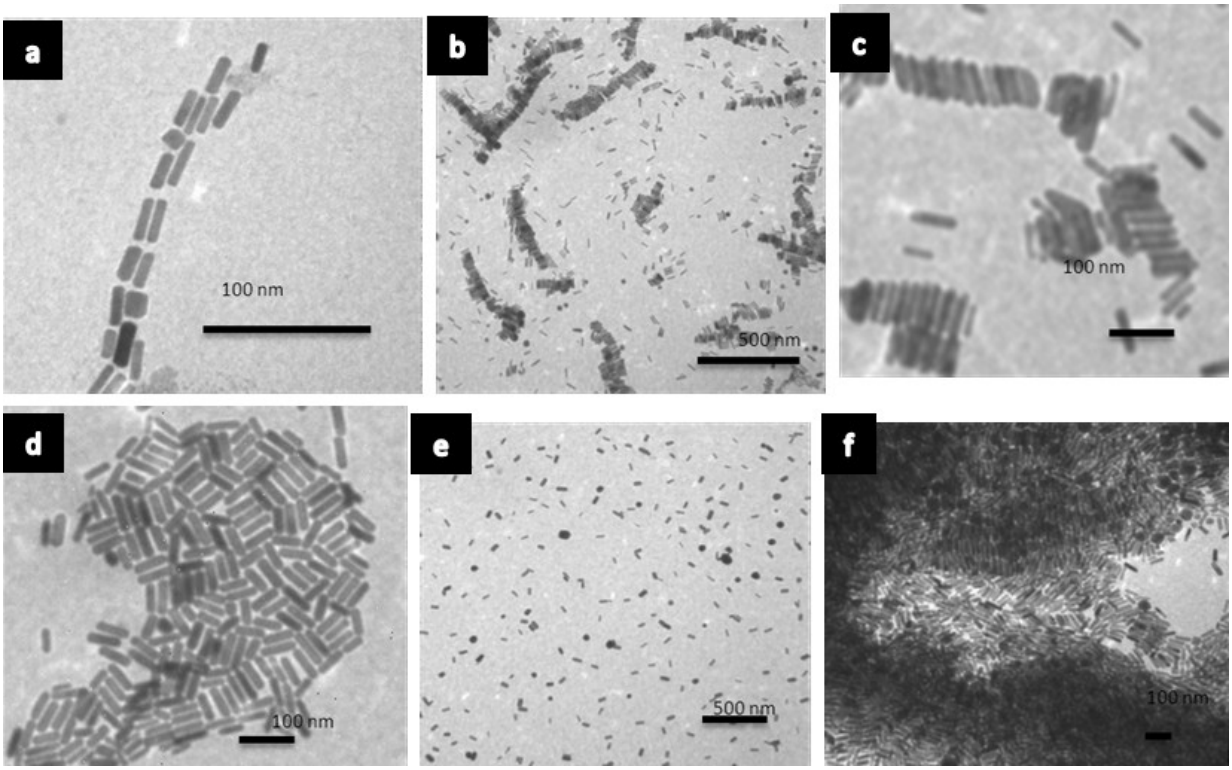

Figure 18. TEM images of self-assembled Au nanorods.

We successfully self-assembled Pt nanocatalysts into two-dimensional nanostructures by impregnation into Nafion membrane by an electrostatic approach (Figure 19).[41] SEM was used to characterize the self-assembly, distribution and topography of the Nafion polymer films embedded with nanoparticles. Based on their properties (surface charge, size, shape), the nanoparticles showed different dispersion properties in the Nafion membranes. The ability to precisely self-assembly Pt nanoparticles onto Nafion film allows for direct contact and maximum exposure of all active Pt catalysts sites. This resulted in efficient utilization of the Pt surface that can be further tailored to achieve desired catalytic activities while significantly reducing precious metal loading. This approach is expected to efficiently block the methanol crossover through the Nafion electrolyte membrane and enhance the performance of direct methanol fuel cells.

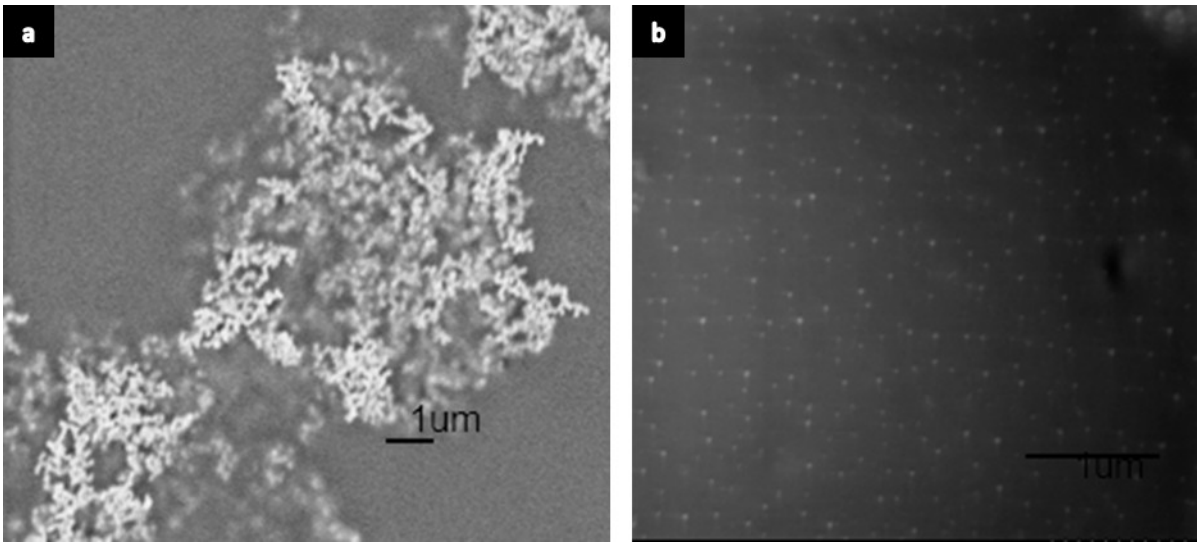

Figure 19. SEM images of (a) aggregated hollow Pt nanospheres (20 nm) and (b) well dispersed hollow Pt nanospheres (20 nm) in Nafion membranes.

Improved bacterial extracellular electron transfer was demonstrated by surface modification with nanomaterials onto solid electrodes. Microbial fuel cells (MFCs) utilize bacteria to generate electricity (electrogenic bacteria) as a result of natural microbial conversion of organic compounds. In this type of bioreactor, an electrode accepts electrons from actively metabolizing microorganisms. Optimized electron transfer reactions, including current production and electron transfer rates are required for the best performance of MFCs. Immobilization of active biofilms onto electrodes or immobilization of electron shuttles increases the overall efficiency and durability of the MFC. One drawback is that the kinetics of electron transfer can be impeded by these approaches[42,43] because electrodes are limited to a monolayer of electrogenic bacteria or electron shuttles. Immobilized cells in a conductive matrix will improve the overall electron transfer efficiency at the electrode. One approach to achieve this goal is through the supplementation of the bacterial surfaces with electroactive and conductive nanomaterials. This modification to bacterial surfaces is expected to increase electron transfer rates and overall current production. To demonstrate the potential for modification of bacterial cultures with nanomaterials, we incorporated gold nanorods with an electrogenic bacterial culture and monitored the electrochemical behavior at the cell surface.

To demonstrate improved electron transfer processes from electrogenic, latex-immobilized bacteria to electrodes, we began by exploiting the electrochemically active microbial polymer, pyomelanin.[44,45] This humic-type polymer, produced by some electrogenic bacteria is associated with the bacterial surface[46] and enhances electron transfer to electrodes.[44,45] Because of the surface sorbing properties of pyomelanin, it can be added to a wide variety of bacterial species to improve extracellular electron transfer behavior, either by supplementing culture media or through genetic manipulation.[44,45] The kinetics of this reaction can be controlled by the thickness of the polymer on the microbial cell surface.[44] The metal chelating properties of pyomelanin[45,47] were also exploited in this study for the incorporation of Au nanorods on the cell surface in order to further improve electron transfer behavior at the electrode.[48] In this study, a strain of pyomelanin over-producing mutants was used to demonstrate the possibility of electron transfer to electrodes by bacteria immobilized onto a graphite electrode. Cyclic voltammograms

(100 mV/s, scan rate) (Figure 20) demonstrated an increased current response by the culture with surface sorbed Au nanorods compared to the culture without Au nanorods. In addition, the rate of electron transfer, as demonstrated by the decrease in separation between oxidation and reduction peaks, was increased by the Au nanorods compared to the data without Au nanorods. The coherent collective oscillation of electrons on Au nanorods surfaces are known to be responsible for such electron transfer enhancements.[49] Au nanorods dispersion was not optimized in our preliminary study based on the clumping observed in Figure 20 (inset). A more homogeneous dispersion of Au nanorods in association with electrogenic bacteria is expected to further improve bacterial extracellular electron transfer to an electrode.

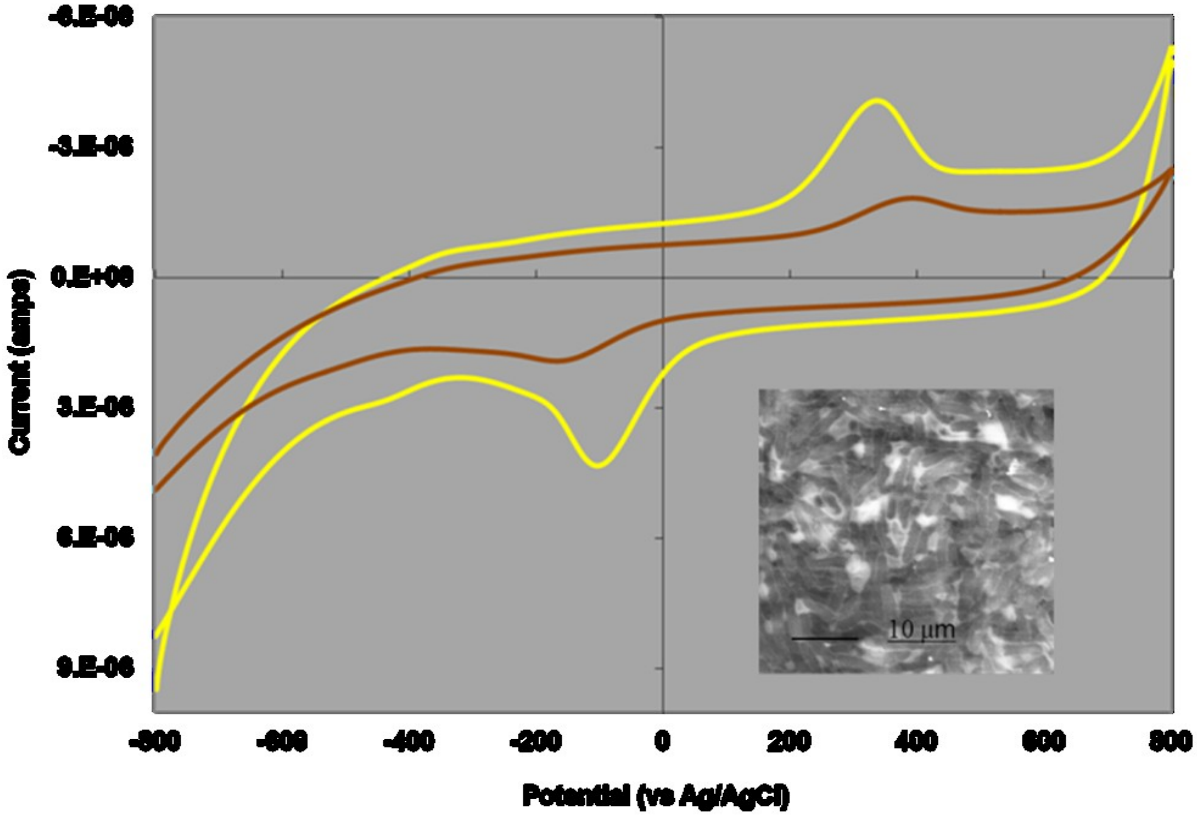

Figure 20. Improved electron transfer at the microbe surface with addition of gold nanorods. 100 mV/s cyclic voltammetry scans demonstrated that the oxidation current peaks (up) and concomitant reduction current peaks (down) increased when nanorods were sorbed to bacterial surfaces (yellow lines). The decrease in the separation between oxidation and reduction peaks of samples with nanorods compared to that without (brown lines) indicates that nanorods also increase the rate of electron transfer between bacteria immobilized onto the electrode surface. Inset is an electronmicrograph of nanorods (white electron dense material) associated with electrogenic bacteria used in this study.

4.3. Three-dimensional nanostructures:

Ordered arrays of one-dimensional nanostructures fabricated by the oblique angle deposition (OAD) method was developed by Zhao's group. For example, using two consecutive glancing angle depositions (GLAD) at different deposition angles and with different materials, a WO_3-core TiO_2-shell nanostructure has been fabricated.[50] This versatile method allows for controlled growth of both the WO_3 "core" as well as the TiO_2 "shell", which maximizes the interfacial area between the two materials, but also optimizes the area of TiO_2 that is in contact with the solution. The photocatalytic enhancement of these core-shell novel structures was up to 70 times over amorphous single layer TiO_2 thin films, 13 times enhancement over crystalline (anatase) TiO_2 thin films, and 3 times enhancement over c-TiO_2/a-WO_3 two-layer thin films, with much less (85% less) the load of TiO_2. These structures also show strong white light responses.[50]

This procedure was also used to prepare sensitive, reproducible, and uniformly aligned Ag nanorod (AgNR) substrate arrays for SERS detection.[21] By exposing the supported Ag nanorod structures to Au^{3+} ions, significant morphological and compositional changes occur. The porosity of the Au layer and the content of Ag decrease with reaction time (Figure 21).

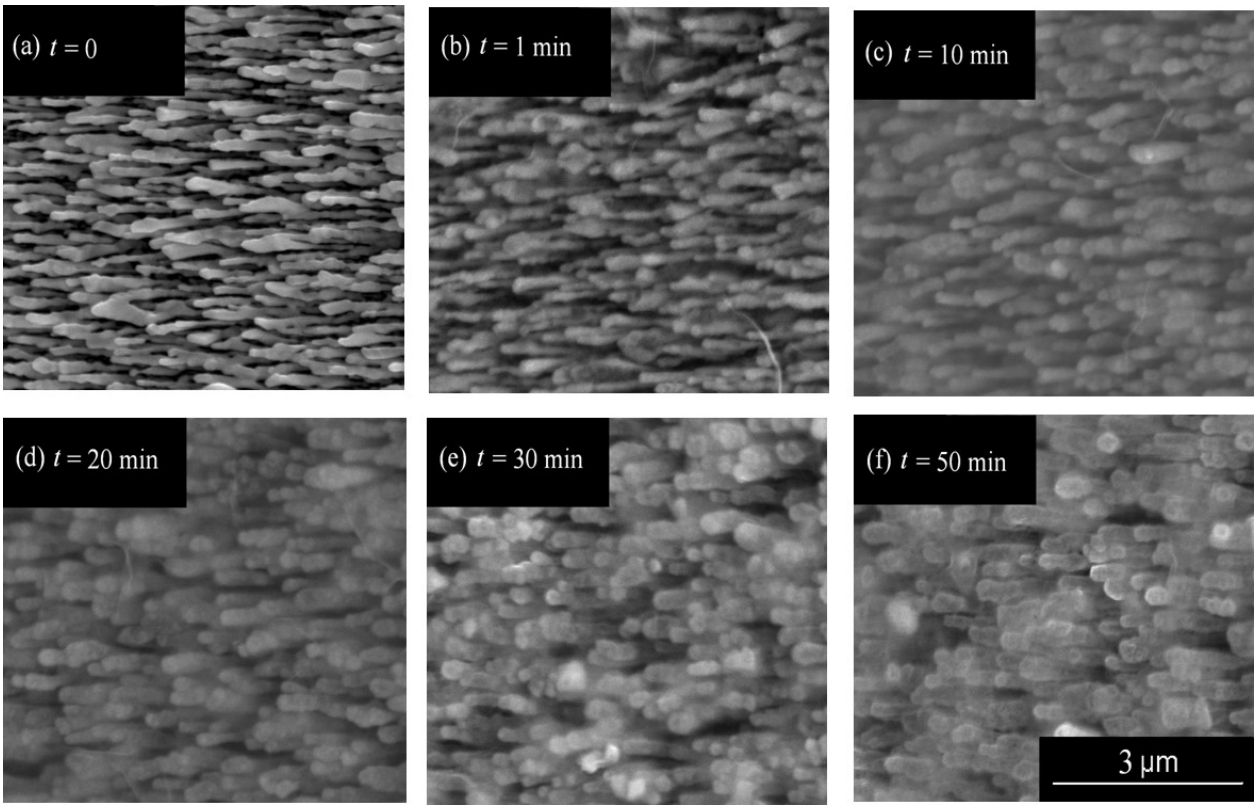

Figure 21. SEM images of the NR samples before and after the GRR withHAuCl4 for different reaction time t ¼ 0, 1, 10, 20, 30 and 50 min, respectively. Scale bar- 3um for a-f. Reproduced by permission of The Royal Society of Chemistry.

Au-modified Ag nanorod are significantly more stable in NaCl solution compared to the as-deposited Ag nanorod. Moreover, when tested for SERS applications the Au-modified Ag nanorod substrate shows an improved SERS sensitivity for air contamination detection (Figure 22). The surface enhanced Raman scattering intensity, tested using 4-mercaptophenol, decreases exponentially with reaction time. This is due to the compositional evolution of the nanostructure from pure Ag to Au–Ag alloy with increasing Au content. However, since the AgNR substrates can achieve a SERS enhancement factor greater than 10^8, the appropriate coating of Au (t < 30 min) could still give a very good enhancement (Figure 22). Coupled with an increased stability compared with the original Ag nanorods, we conclude that the Au nanorods are a good substrate for biological sensing applications that also enhances the detection sensitivity.[21]

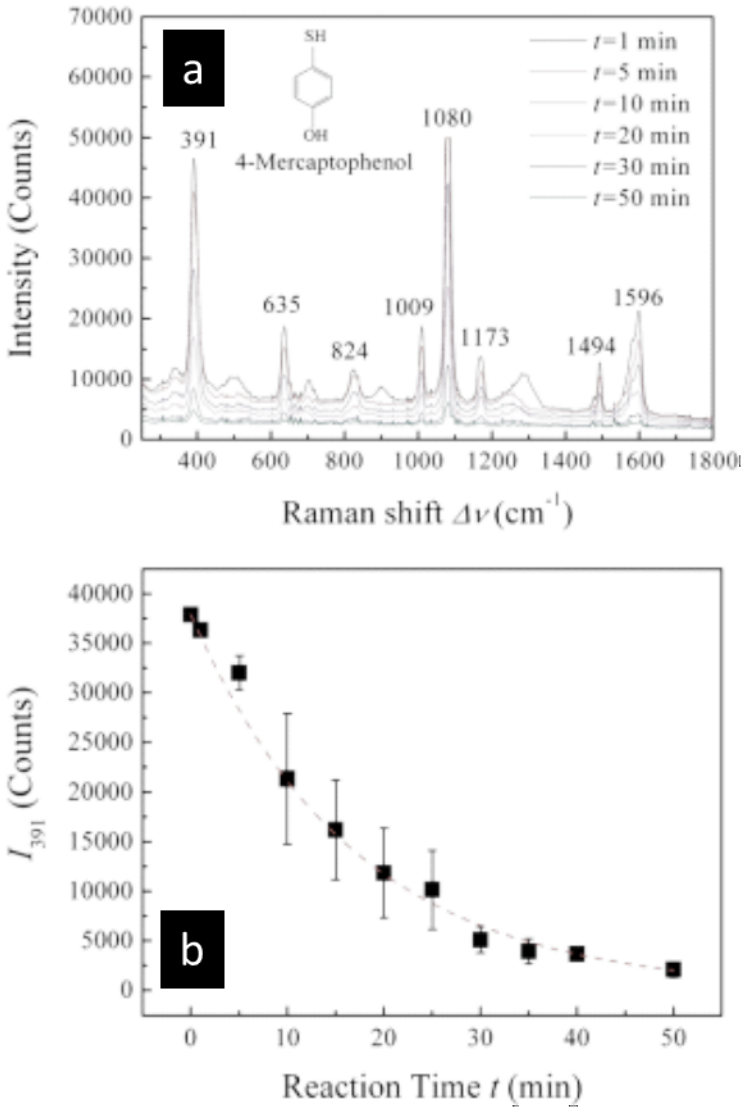

Figure 22. (a) Representative SERS spectra of MPh on the Au-modified AgNR arrays for t = 1, 5, 10, 20, 30 and 50 min, respectively. (b) SERS intensity I_{391} (Δv=391 cm^{-1}) versus reaction time t. The dashed curve is an exponential decay fitting ($I= I_0 exp(-t/k_3)$, k_3= 17.1 ± 0.7min^{-1}, and R^2 =0.9975). Reproduced by permission of The Royal Society of Chemistry

Electron beam lithography is one of the most elegant and powerful methods for three dimensional nanostructure forming. Advanced lithographic techniques have allowed for the fabrication of ordered structures with highly controllable size, shape, and spatial arrangement at the nanoscale. E-beam lithography and atomic layer deposition (ALD) were utilized to fabricate highly ordered arrays of different shaped metallic, e.g. Cr, Pd, Pt, Ag, Au, and Au/Pt nanoparticles (spheres, diamonds, squares, triangles, and rectangles) and/or oxide TiO_2 and SiO_2/TiO_2 nanoparticles supported on Si posts (Figure 22 and 23).

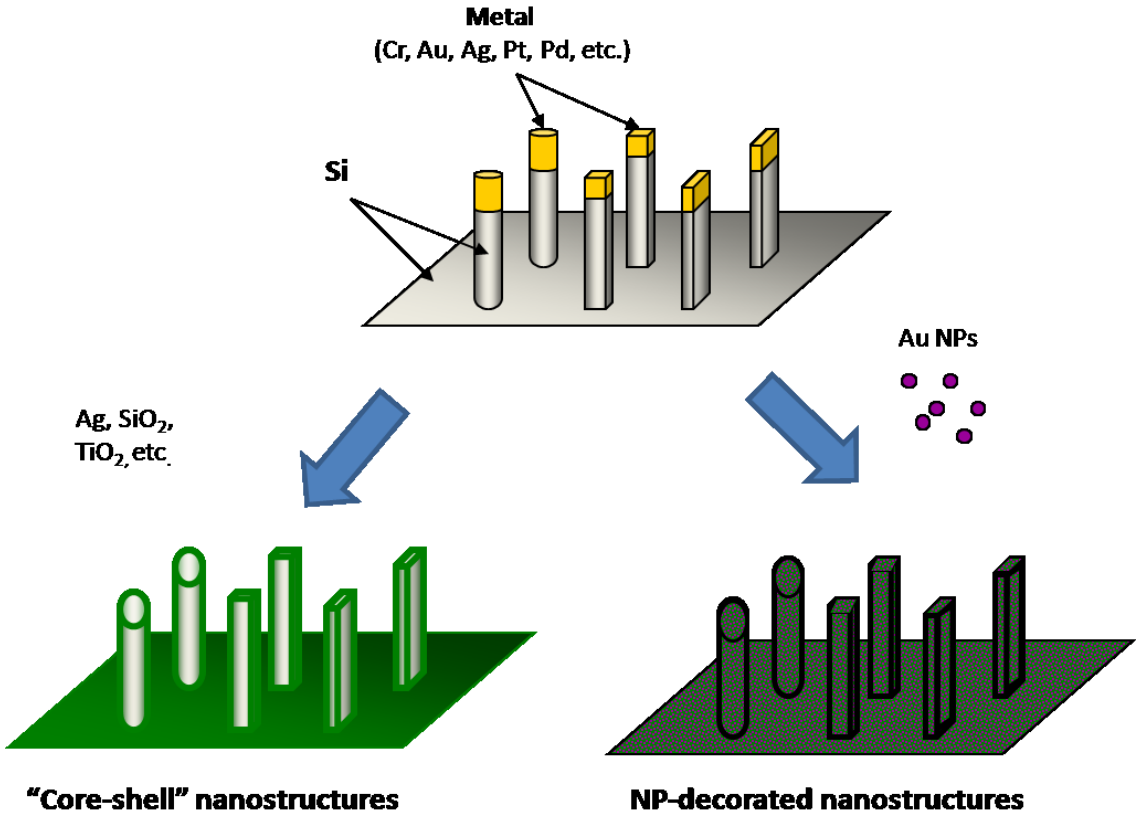

Figure 22. Schematic representation of general lithographic and wet chemical techniques for fabrication of "core-shell" and NP-decorated nanopost arrays.

There is a wide range of potential catalytic applications of such ordered nanostructures. Due to their nanoscale, these arrays have an increased reactive surface area which decreases the amount of precious metal catalyst required in commercial devices. Also, the different shaped

particles may show enhanced catalytic activity compared to the more commonly used spherical or bulk materials. Specifically, the Pt and Pd arrays could be advantageous for fuel cells applications based not only on the on the surface area but also the shape-control alone. In fact, the interesting surface porosity of the Pd nanoparticle arrays produced herein may be a desirable trait for fuel cell applications due to the increased surface area. Bimetallic nanoparticles such as Au/Pt arrays are also promising candidates for DMFC catalysts in that have been shown to exhibit higher stability and catalytic selectivity than their parent metals. Furthermore, noble metals have also been linked to the suppression of CO-poisoning of Pt catalyst surfaces.[51]

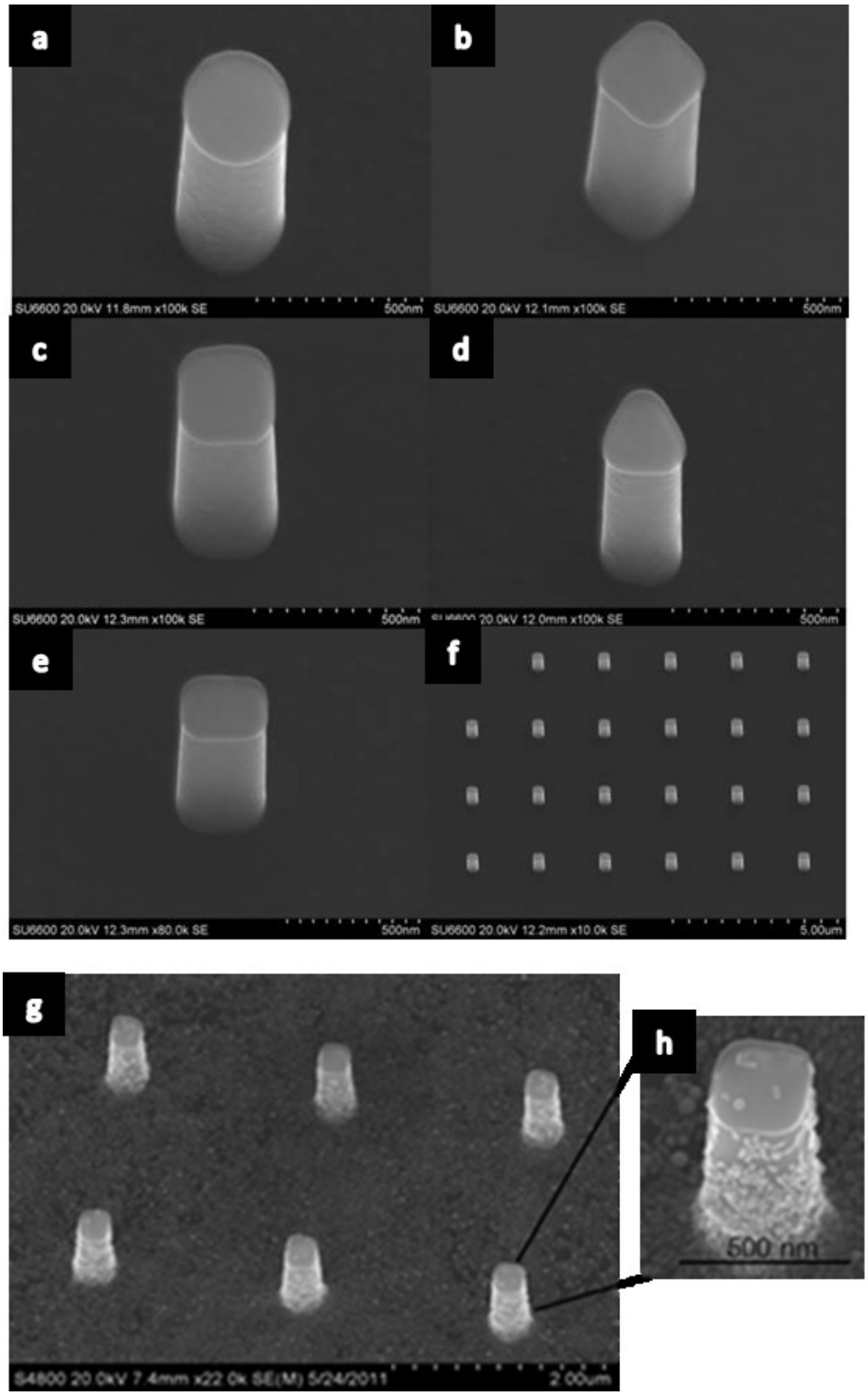
a
b
c
d
e
f
g
h
SU6600 20.0kV 11.8mm x100k SE
500nm
SU6600 20.0kV 12.1mm x100k SE
500nm
SU6600 20.0kV 12.3mm x100k SE
500nm
SU6600 20.0kV 12.0mm x100k SE
500nm
SU6600 20.0kV 12.3mm x80.0k SE
500nm
SU6600 20.0kV 12.2mm x10.0k SE
5.00um
S4800 20.0kV 7.4mm x22.0k SE(M) 5/24/2011
2.00um
500 nm

Figure 23. (a-f) SEM images of TiO_2- and SiO_2/TiO_2-coated nanopost arrays and (g, h) AuNR-decorated SiO_2/TiO_2 nanoarrays.

Titanium dioxide photocatalysis has also received widespread attention as a means for harnessing solar energy to treat polluted water. Much of the emphasis is being placed on destroying volatile organic compounds that are found in contaminated groundwater.[52] TiO_2 it is also well known as an efficient photocatalyst at ultraviolet wavelengths for use in hydrogen production, self-cleaning, and solar cells. Titania has been considered the most appropriate candidate for photocatalytic processes due to its powerful oxidation capability, superior charge transport, and corrosion resistance. Additionally, TiO_2 is inexpensive, has reasonable activity, and is abundant. Despite these attributes, the efficiency of TiO_2 for photovoltaic and photocatalytic applications is severely limited by its large band gap (~3.2 eV) and rapid charge carrier recombination dynamics which means that anatase titania can use less than approximately 1% of the solar spectrum.[53] Thus, it is more desirable to use visible light as the energy source for photovoltaics and photocatalytic applications. Numerous strategies have been employed to sensitize TiO_2 to lower energy light (in order to utilize a larger region of the solar spectrum including surface modification with organic molecules (dyes), doping with various metals and non-metals, coupling to narrow band gap semiconductors, band gap modification through oxygen deficiencies, and controlling the size, shape, and spatial structuring of semiconductor particles.

Another attempt to sensitize TiO_2 to visible light, is using noble metal arrays functionalized with photocatalytic materials. When noble metal nanoparticles are embedded or associated with semiconductor surfaces they have been shown to improve the photocatalytic activity of the material. When an electron is excited from the valence band to the conduction band of a semiconductor upon irradiation by a specific energy, the noble metal acts as a sink for the photo-induced charge, essentially capturing the electron. This helps to prevent recombination of the photo-generated electron-hole pairs in the semiconductor material and thus improve its overall photoelectrochemical performance.[54]

Metallic nanoparticles exhibiting localized surface plasmon resonance (LSPR) have led to significant enhancements in thin film and nanostructured solar technologies. These surface plasmons essentially act as optical antennas that, at specific frequencies, can create intense electromagnetic fields near the metal causing enhanced light absorption and scattering effects on the semiconductor surface.[55,56,57] Recently, Thomann *et al.*[58] have demonstrated that the plasmonic effects of Au nanoparticles could significantly enhance water splitting in a prototypical iron oxide (Fe_2O_3) photoanode.

We have successfully fabricated novel TiO_2, SiO_2-TiO_2, TiO_2-Au and SiO_2-TiO_2-Au composite nanomaterials for photocatalytic applications. Electron-beam lithography and atomic layer deposition allowed for tremendous size and shape control of the metal oxide nanoparticles. A wet chemical self-assembly approach was successfully employed to couple anisotropic Au nanoparticles to the TiO_2 and SiO_2-TiO_2 arrays as shown in Figure.

Photodegradation studies of a model analyte, methyl orange, were conducted on these nanoarrays to evaluate their potential photocatalytic properties. The SiO_2/TiO_2-coated nanostructures showed significant activity toward the photodegradation of methyl orange (10 uM solution) in UV light with up to 52% MO degradation in 6 hours (Figure 24).[53] The MO degradation is shown in the UV-Vis absorption spectra over this exposure period in Figure. A

blank SiO_2/TiO_2 control (with no nanopatterned array) showed almost no degradation of MO under UV illumination which clearly indicates the importance of nanostructuring of TiO_2 on its catalytic performance. Au nanorod-functionalized TiO_2-coated post arrays were also tested for photocatalytic activity under visible illumination. The MO control solution and ordered titania post array with no Au nanorods showed essentially no MO degradation in visible light over the same exposure period. However, some degradation (up to ~6%) was observed under visible light when exposed to the Au-functionalized arrays which clearly indicates that the AuNRs play an essential role in sensitizing TiO_2 to visible light. Only a small percentage of the TiO2 surface (~5%) was coated in AuNRs, therefore, optimization of the wet chemical synthesis is necessary to increase the catalytic activity in visible light.

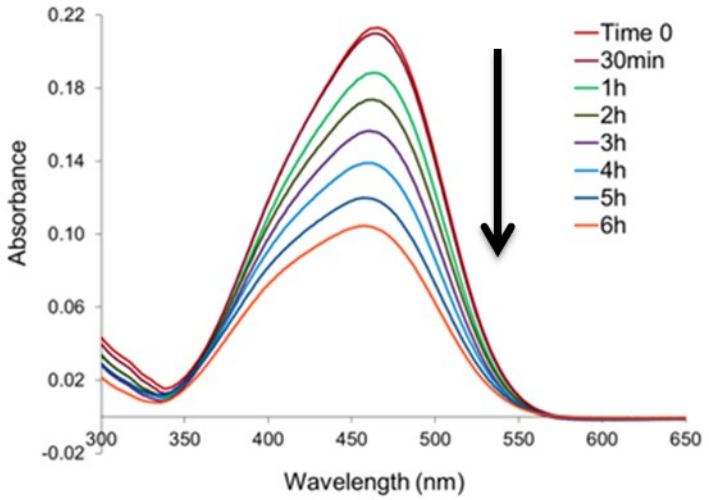

Figure 24. UV-Vis spectra of 10uM methyl orange solution upon exposure to UV light in the presence of a SiO_2/TiO_2-coated nanopost array.

Three dimensional nanostructured photoelectrodes for DSCs have proven to be a promising technique for combatting the charge transfer issues prevalent in traditional nanocomposite films. Such structures including nanowires, nanotubes, nanorods, nanobelts, and nanofibers placed strategically perpendicular on the supports provide a direct pathway for electron transport between the photon-excited surface/dye and the conducting film of the electrode.[59,60,61] The electron transport in photoelectrodes composed of these arrays can occur up to 100 times faster than the corresponding nanocrystalline or nanoparticle-based films.[62]

A series of experiments and theoretical simulations was carried out to show that (1) metallic nanoparticles can indeed enhance the photocurrent of a material when incident light is near the surface plasmon resonance of the nanoparticles and (2) to confirm that this enhancement is a characteristic of plasmonic structures and does not arise from other chemical/physical effects.58 Noble metal nanoparticles (particularly Au and Ag) have also been used extensively to couple to wide bandgap semiconductors like TiO_2 in order to sensitize them to lower energy

light. These nanoparticles exhibit localized surface plasmon resonance (LSPR) in the visible and near-IR regions of the solar spectrum which is a collective oscillation of surface electrons in metallic materials.[6,11,13] The frequencies that these plasmons resonate at are highly dependent on the size, shape, and composition of the nanoparticle so they can be easily tailored for a specific wavelength or function.[9,11,13] When coupled to semiconductor materials, the plasmonic particles create band gap defect sites (or intermediate bands) allowing for electronic transitions from the valence band to the conduction band of the semiconductor under sub-band gap illumination.[63]

In 2005 and 2006, Yu and coworkers[64,65] showed that the photocurrent of standard Si-based thin film cells could be improved with the presence of Au nanoparticles on top of the pn junction. This is due to the fact that the depth at which the electric field concentration occurs is on the order of 10's of nanometers which is too short to be of relevance to the pn junction which typically lies 0.2-1um beneath the surface. The concentration of nanoparticles at the pn junction plays an important role in that too few particles will not scatter enough light to make an appreciable difference in photocurrent whereas with too high a concentration the nanoparticles will reflect too much light.[66] Similar enhancements have also been observed in Ag nanoparticle modified Si-based solar cells.[67]

Tatsuma *et al.*[68] and others[69] have demonstrated plasmon-induced charge separation in TiO2 coupled to Au or Ag nanoparticles and applied it to photovoltaics and photocatalysis. Particles exhibiting LSPR absorb light much more strongly than the typical absorber dyes used in DSCs.[55] This would reduce the need for three dimensional TiO_2 nanostructures and large amounts of dye molecules for standard DSCs. Additionally, plasmon-induced charge separation is found to take place where the oscillating electric field is localized, i.e. on edges and corners of particles.[70] This further emphasizes the effect of nanoparticle size and shape on the optoelectronic properties of plasmonic materials.[71] In 2011, an all solid state In/TiO_2/MNPs/ITO solar cell was developed where MNP is Au nanoparticles or Ag nanoparticles and ITO is indium tin oxide coated glass. The metal nanoparticles were produced by either vapor deposition or electrodeposition onto the ITO electrode. Though simple and cost-effective, these solid state cells have very low energy conversion efficiencies likely due to the lack of isolation between the TiO_2 and ITO anode as in wet-type cells with a liquid electrolyte.[68]

Li *et al.*[72] recently reported a DSC photoanode consisting of Ag nanoparticle-doped TiO_2 nanofibers fabricated by the electrospinning method. Although the electron lifetime was shorter for the doped nanofibers, the increased diffusion length and faster electron transport along with enhanced light absorption from the plasmonic Ag nanoparticles resulted in a ~25% increase in conversion efficiency as compared to undoped TiO_2 nanofibers. In 2011, Hou *et al.*[73] reported enhanced energy conversion efficiency in DSCs with Au nanoparticle-embedded TiO2 working electrodes. Three different AuNP/dye/TiO_2 configurations were studied in order to find the optimal plasmonic effect from the AuNPs. In two of the configurations, the Au nanoparticles were evaporated onto the surface of the TiO_2 film with a monolayer of Ru-based dye deposited underneath or on top of the AuNPs. The third configuration consisted of a monolayer of the dye deposited on top of an AuNP-embedded TiO_2 film. The structure with embedded Au nanoparticles exhibited a marked increase in photocurrent compared to a standard DSC with a subsequent conversion efficiency increase from 0.94% to 2.28%. The two configurations in which Au nanoparticles were deposited on top of the TiO_2 film showed decreased performance compared to the standard DSC. This is due to either the decreased dye surface area exposed to incident light or a decrease in the TiO2 surface area in contact with the light-absorbing dye.

Conclusions

Rational assemblies of metallic nanoparticles in one-, two- or three dimensions have become an increasingly attractive method for developing nanoscale architectures for electronics, sensing, and photocatalytic applications. Nanoscale architectures often exhibit improved physical and chemical properties over their single-component counterparts, and hence are potentially useful in a broader range of applications. This book chapter summarized recent advances in the design and fabrication of 1D, 2D and 3D architectures. Metallic nanoparticles, particularly of silver, gold, and platinum, or a combination of those metals (Ag-Pt, Au-Pt, Au-Ag), various oxides (TiO_2, SiO_2) or carbon nanotubes are used as templates for creation of complex and ordered nanomaterials with tailored and tunable structural, optical and surface properties. Bottom up and top down approaches are the main key concepts that allows production of nanomaterials and nanoarchitectures with precisely defined properties and functions.

Representative applications pertinent to chemical sensing via SERS and energy related application of these advanced nanoarchitectures is described. Ultimately, the promise of these technologies and applications depends on the scientist's ability to deliberately manipulate matter at atomic levels and produce nanoscale materials production in large quantities.

References

[1] Hunyadi, S.E. "*Nanoengineered Materials: Synthesis, design, functionalization and chemical sensing applications*", University of South Carolina, Columbia, SC, **2007**.

[2] Feynman, R.P. "There's Plenty of Room at the Bottom", 1959, http://www.zyvex.com/nanotech/feynman.html.

[3] Mallouk, T. E.; Kovtyukhova, N. I. Chem. Eur. J. 2002, 8, 4354-4363; Law, M.; Sibuly, D. J.; Johnson, J. C.; Goldberger, J.; Saykally, R. J.; Yang, P. Science **2004**, 305, 1269-1273.; Maier, S. A.; Brongersma, M. L.; Kik, P, G.; Meltzer, S.; Requichia, A. A. G.; Atwater, H. AdV. Mater. **2001**, 13, 1501-1505.; Maier, S. A.; Kik, P. G.; Atwater, H. A.; Meltzer, S.; Harel, E.; Koel, B. E.; Requichia, A. A. Nature Mater. 2003, 2, 229-232.; Fan, H.; Lu, Y.; Stump, A.; Reed, S. T.; Baer, T.; Schunk, R.; Perez-Luna, V.; Lopez, G. P.; Brinker, C. J. Nature 2000, 405, 56-60.; Gao, H. J.; Ji, B. H.; Jager, I. L.; Arzt, E.; Fratzl, P. Proc. Natl. Acad. Sci. U.S.A. 2003, 100, 5597-5600.; Ji, B. H.; Gao, H. J. J. Mech. Phys. Solids 2004, 52, 1963-1990.; Katz, E.; Willner, I. Angew. Chem., Int. Ed. Engl. 2004, 43, 6042-6108.; Schultz, D. A. Curr. Opin. Biotechnol. 2003, 14, 13-22.; Salem, A. K.; Searson, P. C.; Leong, K. W. Nature Mater. 2003,2, 668-671.

[4] Clarkson, T. *Environmental Health Perspectives*, **1995,***103(1)*, 9-12.

[5] Faraday, M. P*hilos. Trans. R. Soc. London*, **1857**, 147.

[6] Murphy, C.J.; Gole, A.M.; Hunyadi, S.E.; Orendorff, C.J., *Inorg. Chem. (Forum Article)*, **2006**, *45*, 7544-7554.

[7] Haruta, M., *The Chemical Record*, **2003,** 3, 75–87.

[8] Murphy, C.J.; Gole, A.M.; Hunyadi, S.E.; Stone, J.W.; Sisco, P.N.; Alkilany, A.; Kinard, B.E.; Hankins, P. *Chem. Comm. (Feature Article),* **2008**, *4*, 554-557.

[9] Hunyadi Murph, S.E.; Murphy, C.J.; Colon-Mercado, H.; Torres, R.; Heroux, K.; Fox, E.; Thompson, L.; Haasch, R. ***J.*** *Nanoparticle Research*, **2011**, 13, 6347-6364.
[10] Murphy, C.J.; Sau, T.K.; Gole, A.M.; Orendorff, C.J.; Gao, J.; Gou, L.; Hunyadi, S.E., Li, T. *J. Phys. Chem. B,* **2005**, *109*, 13857-13870.
[11] Hunyadi, S.E.; Murphy, C.J., *J. Mater. Chem*.; Special Issue: Anisotropic Nanoparticles **2006**, *16*, 3929 - 3935.
[12] Hunyadi Murph, S.E.; Jacobs, S.; Siegfried, M.; Hu, T.; Serkiz, S.; Hudson, J. *J. Nanoparticle Res.*, 2012, 14, 658-659.
[13] Hunyadi Murph, S.; Serkiz, S.; Fox, E.; Colon Mercado, H.; Sexton, L.; Siegfried, M. *Fluorine-Related Nanoscience with Energy Applications, ACS Symposium Series*, Volume *1064*, Chapter 8, **2011**, 127-163.;
[14] Sirimahachai, U.; Ndiege, N.; Chandrasekharan, R.; Wongnawa, S.; Shannon, M. A. *J. Sol-gel Sci. Techn.* **2010**, *56*, 53-60.
[15] Haruta, M. *Catal. Today*, **1997**, *36*, 153-166
[16] Jogi, I.; Pars, M.; Aarik, J.; Aidla, A.; Laan, M.; Sundqvist, J.; Oberbeck, L.; Heitmann, J.; Kukli, K. *Thin Solid Films*. **2008**, *516*, 4855-4862.; Matthews, A. *American Mineralogist.* **1976**, *61*, 419-424.
[17] Martin, N.; Rousselot, V.; Rondot, D.; Palmino, F.; Mercier, R. *Thin Solid Films.* **1997**, *300*, 113-121.
[18] Hunyadi, S.E.; Murphy, C.J. *J. Phys. Chem. B*, **2006**, *110*, 7226 -7231.
[19] Feldheim, D.L., Foss, C.A., Jr., "*Metal Nanoparticles: Synthesis, Characterization and Applications*", **2002**, Eds. Marcel Dekker: New York.

[20] Bhadra, D.; Bhadra, S.; Jain, S.; Jain, N. K. *Int J Pharm*. **2003**, *257*, 111-124.
[21] Song, C.; Abell, J.; He, Y.; Hunyadi Murph, S.E.; Cui, Y.; Zhao Y *J. Mater. Chem.,* **2012**, 22, 1150-1159.
[22] Fleischmann, M.; Hendra, P.J. ,McQuillan, A.J. *Chem. Phys. Lett.,* **1974,** *26,* 163–166.
[23] Jeanmaire, D. L.; van Duyne, R.P., *J. Electroanal. Chem.,* **1977,** *84*, 1–20.
[24] Albrecht, M., Grant, J. Creighton, A. *J. Am. Chem. Soc.*, **1977,** *99* , 5215–5217.
[25] Nie, S.; Emory, S. R. Science **1997**, 275, 1102-1106.
[26] Nikoobakht, B.; El-Sayed, M.A. *J. Phys. Chem. A*, **2003**, *107*, 3372-3378.

[27] Orendorff, C.J.; Gole, A.; Sau, T.K.; Murphy, C.J. *Anal. Chem.*, **2005***, 77*, 3261-3266.; Orendorff, C.J.; Gearheart, L.; Jana, N.R.; Murphy, C.J. *Phys. Chem. Chem. Phys.*, **2006**, *8*, 165-170.

[28] Kobayashi, Y.; Katakami, H.; Mine, E.; Nagao, D.; Konno, M.; Liz-Marza´n, L. M. *J. Colloid Interface Sci*. **2005**, *283*, 392-396; Bhattacharyya, S.; Saha, S. K.; Chakravorty, D. *Appl*. *Phys*. *Lett*. **2000**, *77*, 3770-3772.
[29] Jain, P.K., Lee, K.S., El-Sayed, I.H., El-Sayed, M.A. *J. Phys. Chem. B*, **2006,** *110,* 7238-7248.
[30] Xia, Y.; Yang, P.; Sun, Y.; Wu, Y.; Mayers, B.; Gates, B.;Yin, Y.; Kim, F.; Ya, H. *Ad*V. *Mater*. **2003**, *15*, 353-389.; Murphy, C.J.; Sau, T. K.; Gole, A. M.; Orendorff, C. J.; Gao, J.; Gou, L.; Hunyadi, S.E.; Li, T. *J. Phys*. *Chem*. *B* **2005**, *109*, 13857-13870.; El-Sayed, M. A. *Acc*. *Chem*. *Res*. **2001**, *34*, 257-264.; Creighton, J. A.; Eadon, D. G. *J. Chem*. *Soc., Faraday Trans*. **1991**, *87*,3881-3891. ; Hu, J. T.; Odom, T. W.; Lieber, C. M. *Acc*. *Chem*. *Res*. **1999**, *32*, 435-

445.; Link, S.; El-Sayed, M. A. *J. Phys. Chem. B* **1999**, *103*, 8410-8426.; uang, Y.; Duan, X. F.; Lieber, C. M. *Small* **2005**, *1*, 142-147.
[31] Hunyadi, S.E.; Murphy, C.J. *J. Phys. Chem. B*, **2006**, *110*, 7226 -7231;
[32] Hunyadi Murph, S.E.; Murphy, C.J. *ChemPhysChem*, submitted.
[33] Yao Yuan; Chaubey Girija S.; Wiley John B. *J. Am. Chem. Soc.*, **2012**, 134, 2450-2452.
[34] Billot, L., Chapelle, M.L., Grimault, A.S., Vial, A.; Barchiesi, D., Bijeon, J.L., Adam, P.M. Royer P. *Chem. Phys. Lett.*, 2006, *422*, 303-307.
[35] C.G. Blatchford, J.R. Campbell and J.A., Creighton *Surf. Sci.*, **1982**, *120*, 435-438.
[36] U. Laor and G.C. Schatz, *J. Phys. Chem*, **76**, (1982), 2888-2899.
[37] Bentzen, M. D.; van Wonterghem, J.; Morup, S.; Thlen, A.; Koch, C. J. *Philos. Mag. B* **1989**, *60*, 169.
[38] Fink, J., Kiely, C.J., Bethell, D., Schiffrin, D.J. *Chem. Mater.*, **1998**, *10*, 922-926.
[39] Nikoobakht, B., Wang, Z.L., El-Sayed, M.A. *J. Phys. Chem. B*, **2000,** *104*, 8635-8640.
[40] Jana, N.R., Gearheart, L.A., Obare, S.O.; Johnson, C.J., Edler, K.J., Mann, S., Murphy, C.J. J. Mater. Chem. 2002, 12, 2909-2912; Jana N.R., *Angew. Chem Int. Ed.* **2004**, *43*, 1536-1540.
[41] Hunyadi Murph, S.E., R.D. Torres *Nanotech,* **2010***, 3,* 777-778.
[42] Wagner, R.C., Porter-Gill, S., Logan, B. E. *AMB Express*. **2012**, In press.
[43] Kochius, S., A.O.Magnusson, F. Hollmann, J. Schrader and D. Holtmann. *Appl. Microbiol, Biotechnol.* **2012***, 93*, 2251-2264.
[44] Turick, C. E., Beliaev, A., Ekechukwu, A.A., Poppy, T., Maloney, A., Lowy. D.A. *Microbiology Ecology* **2009**, *68,* 223-235.
[45] Turick, C.E., Knox, A.S.; Becnel, J.M., Ekechukwu, A.A. and C.E. Milliken Properties and Function of Pyomelanin, Biopolymers, Magdy Elnashar (Ed.), **2010.** ISBN: 978-953-307-109-1, Sciyo, http://sciyo.com/articles/show/title/properties-and-function-of-pyomelanin
[46] Turick, C.E., Caccavo, F. Jr., Tisa.=, L.S. *Microbiol. Let.* **2003,** *220*, 99-104.
[47] Turick, C.E., Knox, A.S., Leverette, C. L. Kritzas, Y.G. J. *Environ. Rad.* **2008,** *99*, 890-899.
[48] Hunyadi Murph, S.E., Murphy, C. J.; Colon-Mercado H.R., Torres, R.D.; Heroux, K.J.; Fox, E.B., Thompson, L.B., Haasch. R.T. **2011.** *J Nanopart Res.* 13:6347–6364.
[49] Kelly, K.L., Coronado, E., Zhao, L.L., Schatz, G.C. *J. Phys. Chem. B ,* **2003**, *107*, 668–77.

[50] Smith, W.; Zhao, Y.-P. *Cat. Comm.* **2009,** 10, 1117; Smith, W.; Zhao, Y. P. *J. Phys. Chem. C* **2008,** *112*,19635; Smith, W.; Zhang, Z. Y.; Zhao, Y. P. *J. Vacuum Science & Technology B* **2007,** *25*, 1875.

[51] Ren, H,; Humbert, M,; Menning, C. *Appl. Catal. A,* **2010**, *375*, 303-309, Zeng, J,; Yang, J,; Lee, J,; Zhou, W. *J Phys Chem B* **2006**, *110*, 24606-24611.

[52] Badr, Y.; Abd el-Wahed, M. G.; Mahmoud, M. A. *J. Hazard. Mater.* **2008,** *154*, 245-253.
[53] Hunyadi Murph, S.E. *Proc. of SPIE* **2011**, 8109(81090T), 1-11.; Heroux, K.J., Hunyadi Murph, S.E. *J. Mater. Chem.* (in preparation).
[54] Tian, C.; Li, W.; Pan, K.; Zhang, Q.; Tian, G.; Zhou, W.; Fu, H. *Journal of Solid State Chemistry,* **2010,** *183 (11),* 2720-2725.; Subramanian, V.; Wolf, E.; Kamat, P. V. *The Journal of Physical Chemistry B,* **2001,** *105 (46),* 11439-11446.; Arabatzis, I. M.; Stergiopoulos, T.; Andreeva, D.; Kitova, S.; Neophytides, S. G.; Falaras, P. *Journal of Catalysis*, **2003**, *220*, 127-

135.; Anandan, S.; Sathish Kumar, P.; Pugazhenthiran, N.; Madhavan, J.; Maruthamuthu, P. *Solar Energy Materials and Solar Cells,* **2008**, *92*, 929-937.

[55] Ozbay, E. *Science*, **2006**, *311*, 189.
[56] Maier, A. S.; Atwater, H. A. *J. Apple. Phys.* **2005**, *98*, 011101.
[57] Bharadwaj, P.; Deutsch, B.; Novotny, L. Optical Antennas. *Adv. Opt. Photonics* **2009**, *1*, 438.
[58] Thomann, I.; Pinaud, B. A.; Chen, Z.; Clemens, B. M.; Jaramillo, T. F.; Brongersma, M. L. *Nano Lett.* **2011**, *11*, 3440-3446.
[59] Hagfeldt, A.; Boschloo, G.; Sun, L.; Kloo, L.; Pettersson, H. *Chem. Rev.* **2010**, *110(11),* 6595–6663.
[60] Zhang, Q.; Cao, G. *Nano Today* **2011**, *6*, 91-109.
[61] Li, Z.; Rochford, C.; Javier Baca, F.; Liu, J.; Li, J.; Wu, J. *Nanoscale Res. Lett.,* **2010**, *5*, 1480–1486.; Zhu, K.; Neale, N. P.; Miedaner, A.; Frank, A. J. *Nano Lett.,* **2007**,*7*, 69–74.; Lee, K.; Hu, C.; Chen, H.; Ho, K. *Sol. Energy Mater. Sol. Cells,* **2008**, *92*, 1628–1633.; Jiu, J.; Isoda, S.; Wang, F.; Adachi, M. *J. Phys. Chem. B,* **2006**, *110*, 2087–2092.
[62] Cavaliere, S.; Subianto, S.; Savych, I.; Jones, D. J.; Roziere, J. *Energy Environ. Sci.,* **2011**, *4*, 4761–4785.; Law, M.; Greene, L. E.; Johnson, J. C.; Saykally, R.; Yang, P. D. *Nature Mater.* **2005**, *4*, 455-459.
[63] Arabatzis, I. M.; Stergiopoulos, T.; Andreeva, D.; Kitova, S.; Neophytides, S. G.; Falaras, P. *J. Catal.* **2003**, *220*, 127-135.;Anandan, S.; Sathish Kumar, P.; Pugazhenthiran, N.; Madhavan, J.; Maruthamuthu, P. *Solar Energ. Mat. Sol. C.* **2008**, *92*, 929-937.; Kim, S.; Hwang, S.-J.; Choi, W. *J. Phys. Chem B.* **2005**, *109*, 24260-24267.; Zang, L.; Macyk, W.; Lange, C.; Maier, W. F.; Antonius, C.; Meissner, D.; Kisch, H. *Chem. Eur. J.* **2000**, *6*, 379.
[64] Schaadt, D. M.; Feng, B.; Yu, E. T. *Appl. Phys. Lett*. **2005**, *86*, 063106.;

[65] Derkacs, D.; Lim, S. H.; Matheu, P.; Mar, W.; Yu, E. T. *Appl. Phys. Lett*. **2006**, *89*, 093103.
[66] Tsakalakos, L. *Mat. Sci. Eng. R* **2008**, *62*, 175-189.
[67] Pillai, S.; Catchpole, K. R.; Trupke, T.; Green, M. A. *J. Appl. Phys.* **2007**, *101*, 093105.
[68] Takahashi, Y.; Tatsuma, T. *Appl. Phys. Let.* **2011**, *99*, 182110.; Ohko, Y.; Tatsuma, T.; Fujii, T.; Naoi, K.; Niwa, C.; Kubota, Y.; Fujishima, A. *Nature Mater.* **2003**, *2*, 29.; Naoi, K.; Ohko, Y.; Tatsuma, T. *J. Am. Chem. Soc.* **2004**, *126*, 3664.;[Tian, Y.; Tatsuma, T. *Chem. Commun.* **2004**, 1810.; Tian, Y.; Tatsuma, T. *J. Am. Chem. Soc.* **2005**, *127*, 7632.; Sakai, N.; Fujiwara, Y.; Takahashi, Y.; Tatsuma, T. *ChemPhysChem* **2009**, *10*, 766.;Takahashi, Y.; Tatsuma, T. *Nanoscale* **2010**, *2*, 1494.
[69] Chen, Z. H.; Tang, Y. B.; Liu, C. P.; Leung, Y. H.; Yuan, G. D.; Chen, L. M.; Wang, Y. Q.; Bello, I.; Zapien, J. A.; Zhang, W. J.; Lee, C. S.; Lee, S. T. *J. Phys. Chem. C* **2009**, *113*, 13433.; Kowalska, E.; Abe, R.; Ohtani, B. *Chem. Commun.* **2009**, 241.; Kominami, H.; Tanaka, A.; Hashimoto, K. *Chem. Commun.* **2010**, *46*, 1287.; Nishijima, Y.; Ueno, K.; Yokota, Y.; Murakoshi, K.; Misawa, H. *J. Phys. Chem. Lett.* **2010**, *1*, 2031.
[70] Kazuma, E.; Sakai, N.; Tatsuma, T. *Chem. Commun.* **2011**, *47*, 5777.
[71] Burda, C.; Chen, X.; Narayanan, R.; El-Sayed, M. *Chem. Rev.* **2005**, *105*, 1025-1102.; Narayanan, R.; El-Sayed, M. *J. Phys. Chem. B.* **2005**, *109*, 12663-12676.; Narayanan, R.; El-Sayed, M. *Langmuir*. **2005**, *21*, 2027-2033.; Narayanan, R.; El-Sayed, M. *J. Phys. Chem. B.* **2003**, *107*, 12416-12424.; Xia, Y.; Xiong, Y.; Lim, B.; Skrabalak, S. E. *Angew. Chem. Int.*

Ed. **2009**, *48*, 60– 103.;Zecchina, A.; Groppo, E.; Bordiga, S. *Chem. Eur. J.* **2007**, *13*, 2440-2460.

[72] Li, J.; Chen, X.; Ai, N.; Hao, J.; Chen, Q.; Strauf, S.; Shi, Y. *Chem. Phys. Lett.* **2011**, *514*, 141–145.

[73] Hou, W.; Pavaskar, P.; Liu, Z.; Theiss, J.; Aykolb, M.; Cronin, S. B. *Energy Environ. Sci.* **2011**, *4*, 4650.